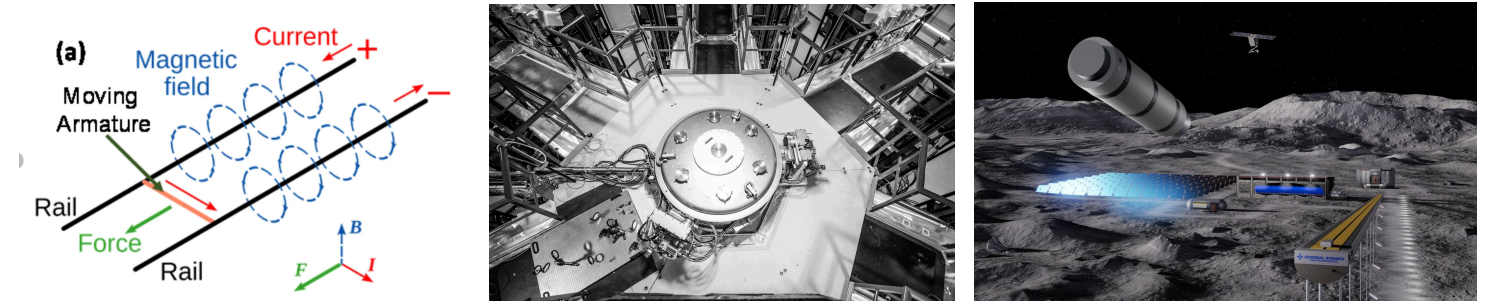


Electromagnetism: The Initial Voltage of a Capacitor Bank and Final Kinetic Energy of Electromagnetic Mass-Driver's Armature

Research Question: How does altering the Initial Voltage (V : 75, 150, 225, 300, 375, 450, 525, 600, 675, 750) of a Capacitor Bank affect the Final Kinetic Energy (J) of the Armature of an Electromagnetic Mass-Driver measured in Finite-Element-Analysis simulation (LS-DYNA)?

1 Introduction



Electromagnetic Mass-drivers use Lorentz force to accelerate an armature to high speeds. Lorentz force arises when current in parallel conductors generates magnetic fields, pushing the armature (Figure-1). Because Lorentz force easily scales with electrical energy rather than being constrained by conventional propellant's chemical properties, mass-drivers can accelerate payloads to extreme theoretical speeds (McFarland & McNab, 2003). This dynamics has attracted interest from firms like *First-Light-Fusion* (First Light Fusion, n.d.) and *US Department-of-Energy* (Los Alamos Scientific Laboratory et al., 1979) for *inertial-confinement-fusion*, where target material is compressed at extreme velocity to initiate Nuclear Fusion (Sandia National Laboratories, n.d.).

Reading Cixin Liu's *Three-Body Problem* (Liu, n.d.), I became intrigued by Fusion. Seeking deeper understanding, I decided to investigate mass-drivers in this paper. Specifically, we examine how increasing a capacitor-bank's initial voltage affects the armature's final kinetic energy. While "higher voltage = more energy" seems straightforward, real-world systems are affected by factors like rail geometry (Lou et al., 2016).

Hence, it's crucial to clarify this relationship to design *inertial-confinement-fusion* mass-drivers effectively. Moving us closer to commercial fusion—an achievement that could address global issues and drastically reduce carbon emissions (IAEA, n.d.). Beyond fusion, mass-drivers also hold promise for aerospace applications, like China's satellite-launch proposals (SCMP, 2024). Due to resource constraints, I employed *Finite-Element-Analysis* LS-DYNA (Ansys Inc., n.d.) instead of constructing a practical mass-driver.

2 Background

Although pulsed-power supplies are typically used for mass-drivers (Lan, 2012) (First Light Fusion, n.d.), for simplicity, this investigation utilizes a **capacitor-bank** only as the mass-driver's power source (Figure-4).

2.1 - Capacitor Bank

A capacitor-bank of capacitance C charged to an initial voltage V_0 stores energy $E_{capacitance}$:

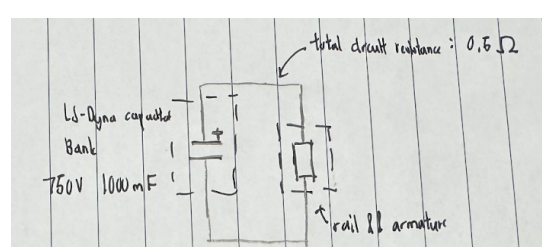


Figure 4: Simulation's Mass-Driver RC Circuit

$$E_{capacitance} = \frac{1}{2} \times C \times (V_0)^2 \quad (1)$$

By Kirchhoff's Voltage Law, completing the circuit triggers an exponential discharge:

$$I(t) = \frac{V_0}{R} e^{-t/RC} \quad (2)$$

where R is circuit resistance, t is time, and $\tau = RC$ is the time-constant.

2.2 - Current Flow and Lorentz Force

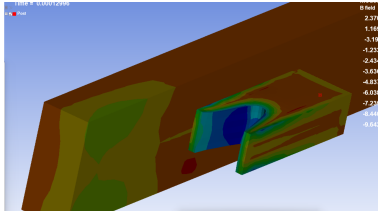


Figure 5: Magnetic Field \mathbf{B} (Y-component)
(Plotted using LS-Dyna)

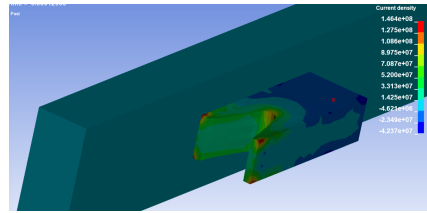


Figure 6: Current Density \mathbf{J} (Z-component)
(Plotted using LS-Dyna)

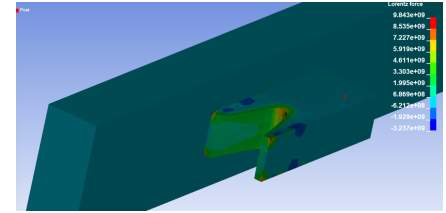


Figure 7: Lorentz Force $\mathbf{F}_{\text{Lorentz}}$ (X-component)
(Plotted using LS-Dyna)

By Ampere's law, current in armature generates a **magnetic field** \vec{B} . The resulting **Lorentz force** \vec{F}_{Lorentz} then arises from the cross product of \vec{J} and \vec{B} (ScienceDirect, 2019):

$$\vec{F}_{\text{Lorentz}} = \vec{J} \times \vec{B} \quad (3)$$

In reality, neither \vec{J} nor \vec{B} remains uniform, because both \vec{J} and \vec{B} vary across the armature's volume (Figure-5 & Figure-6¹), meaning the armature's **total** \vec{F}_{Lorentz} is given by the integral (Waindok, 2017, 153):

$$\vec{F}_{\text{Lorentz}} = \int_{\Omega} (\vec{J} \times \vec{B}) d\Omega \quad (4)$$

where Ω is the armature's volume. This complexity necessitates *finite-element-analysis* for accurate modeling.

2.3 - Armature Acceleration and Kinetic Energy

Summation (4) of \vec{F}_{Lorentz} 's x-component (Figure-7) then accelerates the armature via Newton's Second Law:

$$F = m \times a \quad (5)$$

where m is armature's mass and a its acceleration. Over distance d along the rails, the work done W_{Lorentz} by \vec{F}_{Lorentz} becomes the armature's final kinetic energy E_k :

$$E_k = W_{\text{Lorentz}} = \vec{F}_{\text{Lorentz}} \cdot d \quad (6)$$

2.4 - Hypothesis:

Since Ω is constant, (4) can be simplified to:

$$\vec{F}_{\text{Lorentz}} = k \times (\vec{J} \times \vec{B}) \quad (7)$$

where k is a proportionality constant.

Because of **Ampère's Law** and $\vec{J} \propto I(t)$ (Warnock, 2003, 13), this means $\vec{J}, \vec{B} \propto I(t)$. Thus, (7) can be further simplified to:

$$\vec{F}_{\text{Lorentz}} = k \times [I(t)]^2 \quad (8)$$

¹ Figures 5–7's highlight the distributions of directional-components of \mathbf{J} (z-axis) and \mathbf{B} (y-axis) which, by right-hand rule, generate $\mathbf{F}_{\text{Lorentz}}$ along the x-axis (direction of armature's acceleration in our simulation).

For simplification, we **assume** $\vec{F}_{Lorentz}$ is exerted on the armature only within 2τ . Because after 2τ , only $\sim 1.83\%^2$ of capacitor-bank's initial stored $E_{Capacitance}$ remains, and the armature typically already exits the mass-driver within this timeframe.

By (2), since $\vec{F}_{Lorentz}$ varies over 2τ due to varying $I(t)$. By (8), the average Lorentz Force \bar{F} exerted over rail length $d = 0.1m$ is given by:

$$\begin{aligned}
 \bar{F} &= \frac{1}{2RC} \int_0^{2RC} (k \times [I(t)]^2) dt \\
 &= \frac{k}{2RC} \int_0^{2RC} \left(\frac{V_0}{R} e^{-2t/RC}\right)^2 dt \\
 &= \frac{k}{2RC} \int_0^{2RC} \left(\frac{V_0}{R}\right)^2 \times e^{-4t/RC} dt \\
 &= \left(\frac{V_0}{R}\right)^2 \times \frac{k}{2RC} \int_0^{2RC} (e^{-4t/RC}) dt \\
 &= \left(\frac{V_0}{R}\right)^2 \times \frac{k}{2RC} \times \left[-\frac{RC}{2} e^{-2t/RC}\right]_0^{2RC} \\
 &= \left(\frac{V_0}{R}\right)^2 \times \frac{k}{4} \times (1 - e^{-4})
 \end{aligned} \tag{9}$$

Since $e^{-4} = 0.0183$ is small, we assume it's negligible, simplifying (9) to:

$$\bar{F} = \frac{k \times (V_0)^2}{4R^2} \tag{10}$$

Then, with (6), if we assume 100% of $W_{Lorentz}$ is converted into armature's E_k . This gives us:

$$E_k \approx \frac{k \times (V_0)^2}{4R^2} \times 0.1 \tag{11}$$

Given our derivation (11) shows that $E_k \propto (V_0)^2$, I hypothesise that as capacitor-bank's initial voltage V_0 increases, the final kinetic energy of the armature E_k will increase **quadratically**.

3 Design

3.1 - Choice of Methodology

Although building a practical mass-driver³ was initially attempted, time constraints made it unfeasible. Hence, I used LS-DYNA (Ansys Inc., n.d.) for this investigation instead. LS-DYNA circumvents complications suffered by practical mass-drivers, like soot-buildup (Figure-8) and fabrication inefficiencies, allowing a sharper focus on the research question and also helps develop my FEA-simulation skills—beneficial to my future career in nuclear fusion, where modeling is essential.

I selected LS-DYNA over Ansys-EM because Ansys-EM's licensing costs $\sim \$10,000$ annually (Ding, 2024), whereas LS-DYNA provides a free student version and is more widely used in industry (Ansys Inc., n.d.). While practical mass-drivers normally rely on pulsed-power (Lan, 2012) (First Light Fusion, n.d.), I chose RLC capacitor-bank circuit (Figure-4) for this investigation to avoid pulsed-power's complexities.

I utilized LS-DYNA's exemplar mass-driver model (Ansys Inc., n.d.) because it includes validated meshes, boundary conditions, etc. Further, my initial attempts to simulate my custom design (Figure-9) failed due to contact-penetration errors.

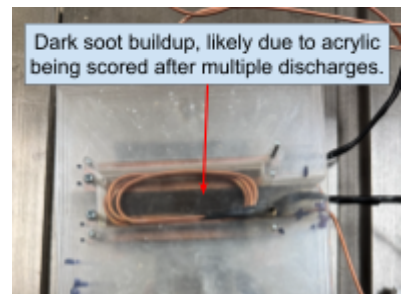


Figure 8: Student's Practical Mass-Driver Post-testing with Soot-buildup

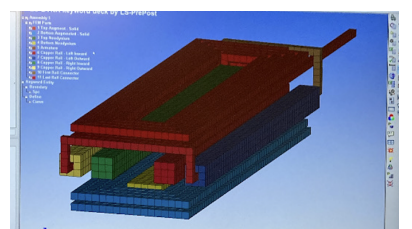


Figure 9: Our Failed Custom Mass-Driver Designed using Autodesk Fusion 360

² By (2), after 2τ , capacitor-bank only retains 13.53% of V_0 . By (1), this means only 1.83% of the initial $E_{Capacitance}$ is retained.

³ If interested, see Appendix-A for procedure of the practical mass-driver I successfully built afterwards.

3.2 - Variables

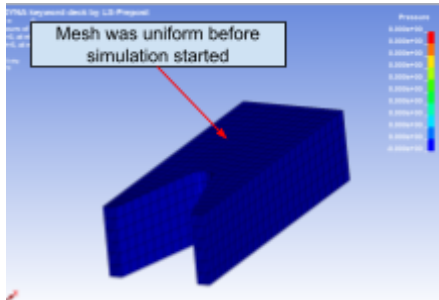


Figure 10: Armature Uniform Mesh Pre-simulation

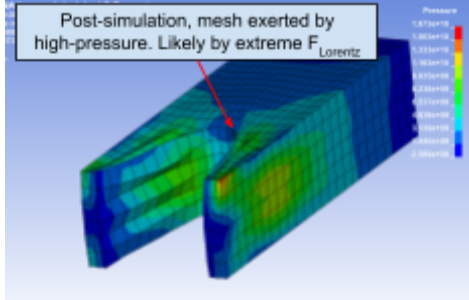


Figure 11: Armature's Mesh Compressed by High Pressure Post-simulation

```

EM error: the EM FER-BEM solver did not converge
Please try to reduce the EM time step
2234 t 9.0007E-05 dt 1.00E+06 write d3plot file
2234 t 9.0007E-05 dt 1.00E+06 write d3plot file
| Error termination
Memory required to complete solution : 215K
Linear Alg dynamically allocated memory: 33M
Additional dynamically allocated memory: 41M
Total: 73M

```

Figure 12: Simulation Failure Error Code

Independent Variable	Initial Voltage of Capacitor Bank V_0 (V)
	V_0 ranged from 75V to 750V (in 75V increments) via “ EM_Circuit ”. This range (75V-750V) was chosen after preliminary tests showed that $V_0 < 75V$ yielded negligible final E_k while $V_0 > 750V$ produced extreme $\vec{F}_{Lorentz}$ which caused mesh collapse (Figure-10 & Figure-11), causing simulation failure (Figure-12). ⁴ 75V incrementation was chosen because it balances between trend-analysis resolution and computational cost. ⁷
Dependent Variable	Final Kinetic Energy of Armature E_k (J)
	Activating “ EM_DATABASE_PART_DATA ”, armature’s E_k is recorded each timestep. Once simulation completes, we record the armature’s final timestep’s E_k from “ EM_PART_DATA_xx.dat ” file. Although LS-DYNA outputs high-precision data (FP-64) (DYNAmore GmbH, n.d.), practical accuracy ultimately depends on chosen timestep size and mesh quality (Boz et al., 2014).

Table 1: Independent and Dependent Variables

Controlled Variables	Impact	Actions taken to Control
Circuit Resistance R & Capacitance C	From (2), modifying R or C impacts $I(t)$, directly affecting $\vec{F}_{Lorentz}$.	We fixed $R = 0.5\Omega$ and $C = 1F$ throughout, ensuring fair test.
Material Properties	Rail and armature’s material properties (Ansys Inc., 2024) determines the armature’s mass, \vec{j} distribution and stress responses, affecting $\vec{F}_{Lorentz}$.	We used LS-DYNA exemplar’s default material settings (density, conductivity, etc.) throughout, ensuring fair test.
Initial Position & Velocity v_0	Altering armature’s initial position or giving it nonzero v_0 could introduce extraneous E_k or reduce the travel distance under $\vec{F}_{Lorentz}$.	We positioned the armature at same starting position with $v_0 = 0 \text{ m/s}$ throughout, ensuring any measured E_k comes solely from $\vec{F}_{Lorentz}$.
Geometry of Rails & Armature	From (4), changes to geometries redistribute \vec{j} and \vec{B} , causing unpredictable $\vec{F}_{Lorentz}$ variations.	We used LS-DYNA exemplar’s default mass-driver geometry throughout.

Table 2: Controlled Variables

⁴ Refining mesh-quality may prevent collapse at higher V_0 . However, at 750V, the armature already reaches Mach 17.5, exceeding *inertial-confinement-fusion* requirements (Wang, 2024), making higher V_0 unnecessary.

Controlled Variables	Impact	Actions taken to Control
Timestep & Mesh Setup	Finer meshes and smaller timesteps improve calculation accuracy but increase computation time (Boz et al., 2014).	We use $timestep = 0.00001s$ and exemplar's default mesh throughout to ensure fair test.
Absence of Atmosphere & Gravity	Including air-resistance and gravity influences armature's net $\vec{F}_{Lorentz}$, potentially masking voltage-related outcomes.	We disabled air-resistance and gravity throughout to focus purely on electromagnetic contribution to E_k .
Armature's Translational & Rotational Constraints	Without constraints, the armature's mesh could penetrate into rails' mesh, causing simulation failure (Watson et al., 2017).	We kept exemplar's default constraints throughout to ensure stable runs.

Table 2 continued: Controlled Variables

3.3 - Procedure

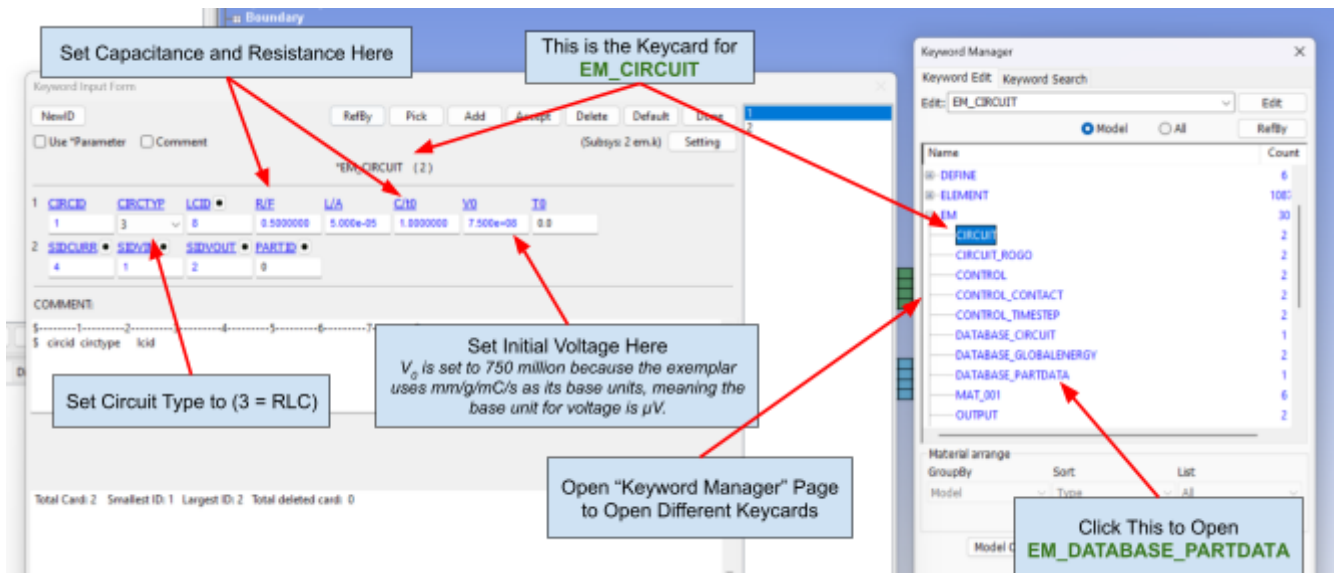


Figure 13: LS-DYNA Keyword Manager

1. Download LS-DYNA and Mass-Driver exemplar file from Ansys' website (Ansys Inc., n.d.).
2. Open exemplar in LS-PrePost (DYNAmore GmbH, n.d.).
3. In “EM_CONTROL_TIMESTEP” (Figure-13), set $timestep = 0.00001s$ and $termination\ time = 0.001s$.
4. In “EM_CIRCUIT”, set circuit type to “RLC” so our mass-driver is powered by a capacitor-bank.
5. Set V_0 to 75V.
6. Activate “EM_DATABASE_PART” which records armature’s E_k every timestep.
7. Execute using LS-Run (Ansys Inc., n.d.).
8. After simulation convergence, open “EM_PART_DATA_xx.dat” to record final E_k .⁵ Optionally use D3Plot for visualization.
9. Repeat step 5-8 for $V_0 = 150, 225, 300\dots 750V$.
10. Repeat step 5-9 six times.

⁵ We omitted overly-technical LS-DYNA settings. If interested, see Appendix-C for our LS-DYNA keycards and example “EM_PART_DATA_xx.dat” file.

3.4 - Calibration

To confirm LS-DYNA's suitability, I consulted literature (Caldichoury & L'Eplattenier, 2012), which demonstrated strong agreement between LS-DYNA's predictions and analytical checks. We ensured high precision by enabling FP-64, reducing rounding uncertainties (DYNAmore GmbH, n.d.). However, certain necessary assumptions—like translational constraints (Table-2)—artificially inflates E_k by removing friction, reducing accuracy⁶.

LS-DYNA solver's inherent stochastic variation introduces random uncertainties (Vogt et al., 2007). We reduce random error by repeating each voltage **seven times**. This also satisfies the standard-deviation outlier test requirement (≥ 5 trials) (Codefinity, n.d.) while remaining computationally feasible⁷.

3.5 - Preliminary Simulations

We tested multiple **termination times** and chose **0.001s**. Shorter durations ended the calculation before the armature exited the mass-driver, whereas longer durations unnecessarily wasted computation after the armature already exited the mass-driver.

We set *timestep* = 0.00001s, where each run took ~ 20 minutes. Smaller timesteps improve numerical accuracy but increase computational cost (Boz et al., 2014). This setting best balanced between accuracy and computational cost.⁷

3.6 - Safety, Environmental and Ethical Considerations

Executing LS-DYNA heats CPU to $\sim 80^\circ\text{C}$, risking fire. We mitigated this with ventilation and temperature checks. Our simulations consumed $\sim 6\text{kWh}$, emitting $\sim 4.5\text{kg}$ of CO₂ (Universiti Malaya, n.d.), raising climate concerns. For future expansions we will use renewable *High-Performance-Computing* (HPCwire, 2024) to lessen this impact.

Mass-drivers share similarities with “railguns”, prompting concerns of militarization. However, real-world railgun programs had largely stalled (Saballa, 2021), implying low immediate risk of weaponization.

We believe this investigation is ethically justified, as it advances the scientific understanding of mass-drivers, which is applied in important avenues like *inertial-confinement-fusion* (Sandia National Laboratories, n.d.)—offering near-unlimited clean energy, solving global issues (IAEA, n.d.)—and cost-effective space launches, like China’s recent proposals (SCMP, 2024).

Finally, we ethically sourced and cited all information used, including LS-DYNA exemplar models and software which were downloaded using valid educational licenses (Ansys Inc., n.d.).

4 Data Collection and Processing

4.1 - Qualitative Observations (Simulation)

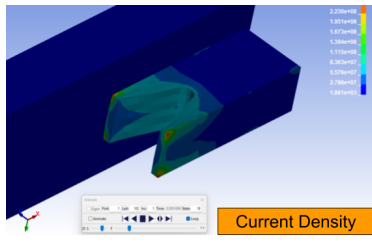


Figure 14: Current Density \mathbf{J} Distributions

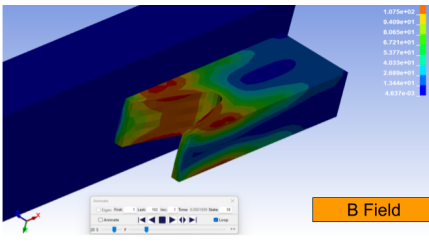


Figure 15: Magnetic Field \mathbf{B} Distributions

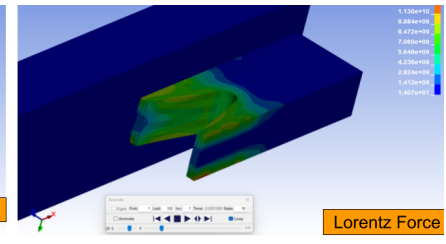


Figure 16: Lorentz Force $\mathbf{F}_{\text{Lorentz}}$ Distributions

Visualising the simulations, D3Plot shows the armature travelling **faster** at higher V_0 . As V_0 increases, both $\vec{\mathbf{J}}$ and $\vec{\mathbf{B}}$ intensifies (Figures-14, Figure-15), yielding a **larger** $\vec{\mathbf{F}}_{\text{Lorentz}}$ (Figure-16). This is consistent with (2), (7), (8).

⁶ These assumptions are acknowledged as limitations in Section-6.

⁷ 20 minutes/run \times 7 repeats \times 10 increments ≈ 23 hours of computation

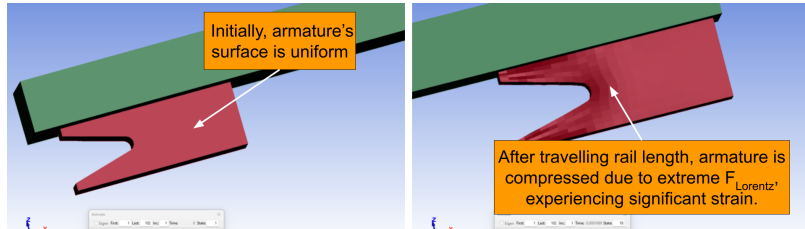


Figure 17: Armature's Mesh Compressed by $\vec{F}_{Lorentz}$

At higher V_0 , the armature appears **compressed** (Figure-17) after traversing rail length, likely due to stronger $\vec{F}_{Lorentz}$. This effect is also observed in Table-1, as strong $\vec{F}_{Lorentz}$ caused mesh collapse and simulation failure (Figure-12).

4.2 - Quantitative Data Analysis

Initial Capacitor Bank Voltage V_0 (V)	Final Kinetic Energy of Armature E_k (J)						
	Trail 1	Trail 2	Trail 3	Trail 4	Trail 5	Trail 6	Trail 7
75	1 702.3	1 791.5	1 833.7	1 740.4	1 769.8	1 811.2	1 842.6
150	6 942.3	7 423.1	6 991.8	7 077.4	7 258.9	6 899.5	7 390.6
225	17 320.4	17 490.1	17 090.9	17 630.2	17 570.5	17 288.3	17 740.0
300	30 491.5	31 942.2	30 220.6	30 688.1	31 540.8	30 310.2	31 104.4
375	45 710.6	47 840.9	46 900.2	45 231.4	48 870.3	46 110.9	48 302.4
450	69 910.8	75 312.6	68 750.3	76 102.2	72 156.9	70 440.6	74 830.1
525	90 810.2	94 503.5	87 190.6	94 221.4	88 893.8	91 630.2	89 016.5
600	120 010.5	114 540.6	123 420.2	117 631.9	111 997.8	119 302.4	122 175.3
675	150 770.2	158 964.9	149 505.6	152 882.6	154 395.1	156 200.4	155 026.8
750	179 540.7	185 210.3	177 617.9	188 405.2	176 552.1	181 340.6	183 120.0

Table 3: Raw Data from LS-DYNA (Obtained from Step 8 of methodology)⁸

All calculations for processing raw data are shown below:

Calculation-1: Average E_k (\bar{E}_k)	Example: $\bar{E}_k = \frac{E_{k_1} + E_{k_2} + E_{k_3} + E_{k_4} + E_{k_5} + E_{k_6} + E_{k_7}}{7}$ $\therefore \bar{E}_k = 181\ 683.8\ J_{(1\ d.p.)}$
Calculation-2: Standard Deviation (σ)	Example: $s = \sqrt{\frac{1}{n-1} \sum_{i=1}^n (x_i - \bar{x})^2}$ $\therefore s = 4\ 227.9\ J_{(1\ d.p.)}$
Calculation-3: Absolute Uncertainty (ΔE_k)	Example: $\Delta \bar{E}_k = \frac{\text{Max} - \text{Min}}{2}$ $\therefore \Delta \bar{E}_k = 5\ 926.6\ J_{(1\ d.p.)}$

Table 4: Calculations Carried Out for Armature's \bar{E}_k at 750V and its associated statistics measures.

⁸ We used double-precision, but we rounded values to one decimal place since higher precision is unnecessary.

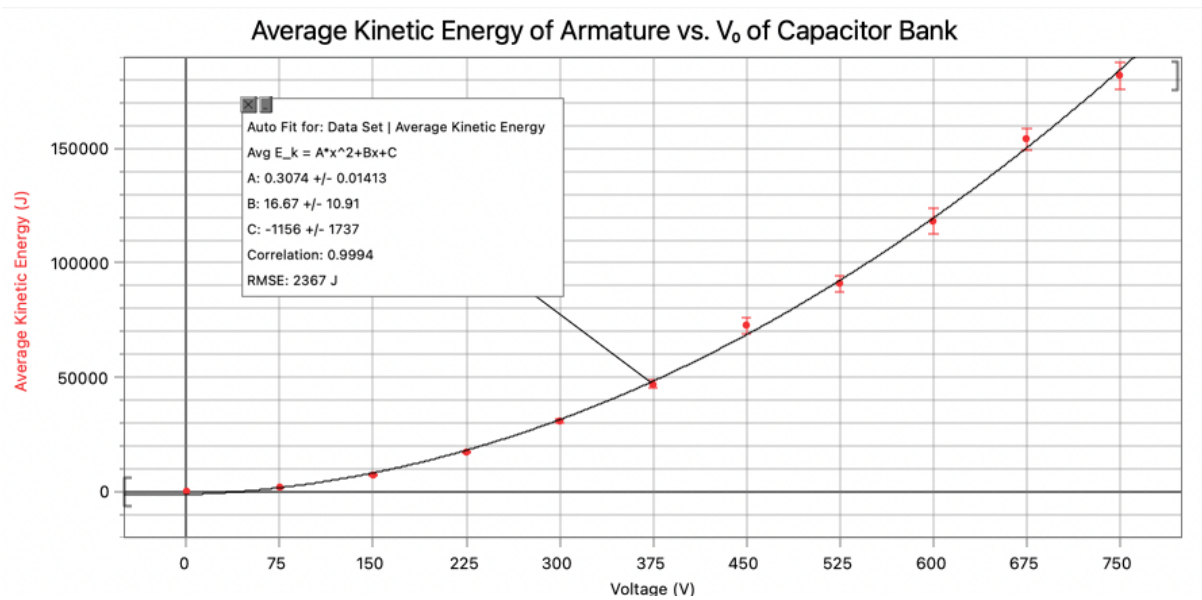
<p><i>Calculation-4: Percentage Uncertainty (\bar{E}_k)</i></p> $\text{Percentage Uncertainty} = \frac{\Delta \bar{E}_k}{\bar{E}_k} \times 100\%$	<p><i>Example:</i></p> $\text{Percentage Uncertainty} = \frac{5926.6}{181683.8} \times 100\%$ $\therefore \text{Percentage Uncertainty} = 3.26\% \quad (3 \text{ s.f.})$
<p><i>Calculation-5: Bounds for determining outliers.</i></p> $\text{Lower Bound} = \bar{E}_k - 3\sigma$ $\text{Upper Bound} = \bar{E}_k + 3\sigma$	<p><i>Example:</i></p> $\text{Lower Bound} = 181683.8 - 3 \times 4227.9$ $\therefore \text{Lower Bound} = 169000.1 J$ $\text{Upper Bound} = 181683.8 + 3 \times 4227.9$ $\therefore \text{Upper Bound} = 194367.5 J$

Table 4 continued: Calculations for Armature's \bar{E}_k at 750V and it's associated statistics measures.

Initial Capacitor Bank Voltage V_0 (V)	Average Final Kinetic Energy of Armature \bar{E}_k (J)	Standard Deviation σ (J)	$\bar{E}_k - 3\sigma$ (J)	$\bar{E}_k + 3\sigma$ (J)	Absolute Uncertainty ΔE_k (J)	Percentage Uncertainty $\frac{\Delta E_k}{\bar{E}_k} \times 100\%$
75	1784.5	50.8	1632.1	1936.9	70.2	3.93 %
150	7140.5	216.0	6492.5	7788.5	261.8	3.67 %
225	17447.2	225.3	16771.3	18123.1	324.5	1.86 %
300	30899.7	653.2	28940.1	32859.3	860.8	2.79 %
375	46995.2	1384.0	42843.2	51147.2	1819.5	3.87 %
450	72500.5	2928.0	63716.5	81284.5	3676.0	5.07 %
525	90895.2	2765.6	82598.4	99192.0	3656.5	4.02 %
600	118439.8	4068.7	106233.7	130645.9	5711.2	4.82 %
675	153963.7	3229.4	144275.5	163651.9	4729.6	3.07 %
750	181683.8	4227.9	169000.1	194367.5	5926.6	3.26 %

Table 5: Summary Table of Processed Data (Calculated Using Operations in Table 4)

Using Logger-Pro (Vernier Science Education, 2018), we graphed:



Graph 1: Final Kinetic Energy of Armature E_k vs. V_0 of Capacitor Bank (Graphed using Table 5)⁹

⁹ Horizontal error-bars are omitted since V_0 is precisely set using EM_CIRCUIT keycard.

4.2.1 - Analysis - Outliers

Outlier test of raw data was performed. Each data point is an outlier if E_k exceeds $\pm 3\sigma$ from \bar{E}_k (Codefinity, n.d.). Since none exceeded these thresholds (Table-5), no outliers were identified, thus all data were retained.

4.2.2 - Analysis - Graph and Uncertainty

Quadratic-fit yields $R = 0.9994$ (Graph-1), indicating a **strong** positive correlation; $R^2 = (R)^2 = 0.9988$ confirms that our data aligns **exceptionally well** with quadratic-regression—strongly supporting our $E_k \propto (V_0)^2$ hypothesis. Coupled with low RMSE, this near-perfect fit allows reliable interpolation across voltages. Although this near-perfect R^2 value seem extraordinary, it's **expected** for a controlled computer simulation.

Graph-1's error-bars remain relatively small across all voltages, with **consistent percentage uncertainty** between 1-5 % (Table-5). This uniformity suggests that most variability arises from minor **simulation stochasticity** (Vogt et al., 2007), which we mitigate by **repeating** each voltage **seven times**. However, because $\frac{\Delta E_k}{E_k} \times 100\%$ is constant, ΔE_k naturally grows at higher V_0 due to \bar{E}_k 's **quadratic scaling**.

4.2.3 - Analysis - Verifying the Quadratic Trend (Linearisation)

To confirm our $E_k \propto (V_0)^2$ hypothesis, we linearize our data's quadratic-regression:

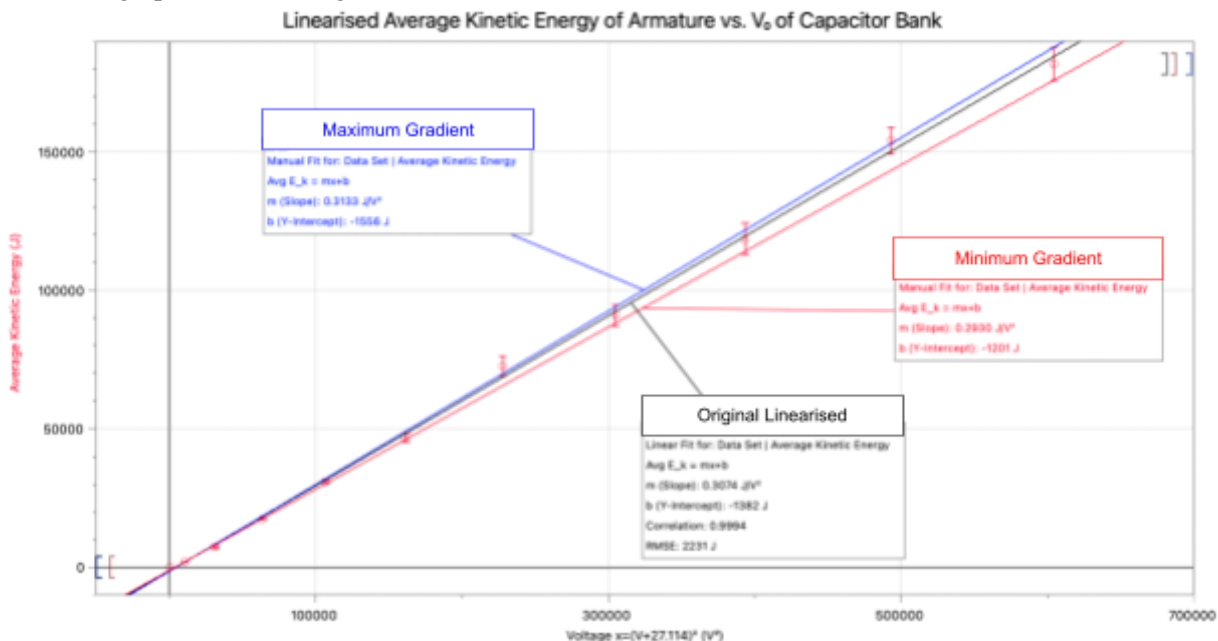
Calculation-6: Linearising Quadratic-Regression Equation	
Completing the Square: $\begin{aligned} y &= ax^2 + bx + c \\ &= a(x^2 + \frac{b}{a}x) + c \\ &= a(x + \frac{b}{2a})^2 + c - \frac{b^2}{4a} \end{aligned}$ Linearised form, where $X = (x + \frac{b}{2a})^2$: $y = aX + (c - \frac{b^2}{4a})$	Linearising our experimental-regression equation: $\begin{aligned} y &= 0.3074x^2 + 16.67x - 1156 \\ &= 0.3074(x^2 + \frac{16.67}{0.3074}x) - 1156 \\ &= 0.3074(x + 27.114)^2 - 1381.99 \end{aligned}$ Hence, the linearised form, where $X = (x + 27.114)^2$: $y = 0.3074X - 1381.99$
Calculation-7: Coordinates of Max-Gradient Linearised Line	
Coordinate 1: $\begin{aligned} X_1 &= (x \text{ value } + 27.114)^2 \\ &= (75 + 27.114)^2 \\ &= 10\,427.3 V^2_{(1 \text{ d.p.})} \end{aligned}$ $y_1 = y \text{ value } - \text{vertical error bar}_1$ $\begin{aligned} &= 1\,784.5 - 70.2 \\ &= 1\,714.3 J_{(1 \text{ d.p.})} \end{aligned}$ Coordinate 2: $\begin{aligned} X_2 &= (x \text{ value } + 27.114)^2 \\ &= (750 + 27.114)^2 \\ &= 603\,906.2 V^2_{(1 \text{ d.p.})} \end{aligned}$ $y_2 = y \text{ value } + \text{vertical error bar}_2$ $\begin{aligned} &= 181\,683.8 + 5\,926.6 \\ &= 187\,610.4 J_{(1 \text{ d.p.})} \end{aligned}$	Coordinate 1: $\begin{aligned} X_1 &= (x \text{ value } + 27.114)^2 \\ &= (75 + 27.114)^2 \\ &= 10\,427.3 V^2_{(1 \text{ d.p.})} \end{aligned}$ $y_1 = y \text{ value } + \text{vertical error bar}_1$ $\begin{aligned} &= 1\,784.5 + 70.2 \\ &= 1\,854.7 J_{(1 \text{ d.p.})} \end{aligned}$ Coordinate 2: $\begin{aligned} X_2 &= (x \text{ value } + 27.114)^2 \\ &= (750 + 27.114)^2 \\ &= 603\,906.2 V^2_{(1 \text{ d.p.})} \end{aligned}$ $y_2 = y \text{ value } - \text{vertical error bar}_2$ $\begin{aligned} &= 181\,683.8 - 5\,926.6 \\ &= 175\,757.2 J_{(1 \text{ d.p.})} \end{aligned}$

Table 6: Calculations for Quadratic Linearization and Max/Min Gradient Slopes

<p>Calculation-9: Max-Gradient Line's Slope m_{max} and Percentage Difference from Best-fit Slope $m_{fit} = 0.3074$</p>	<p>Calculation-10: Min-Gradient Line's Slope m_{min} and Percentage Difference from Best-fit Slope $m_{fit} = 0.3074$</p>
$m_{max} = \frac{y_2 - y_1}{X_2 - X_1} = \frac{187\,610.4 - 1\,714.3}{603\,906.2 - 10\,427.3} \approx 0.3132$ $\frac{\Delta m_{max}}{m_{fit}} \times 100\% = \left \frac{m_{max} - m_{fit}}{m_{fit}} \right \times 100\% = \left \frac{0.3132 - 0.3074}{0.3074} \right \times 100\% = 1.9\% \quad (2 \text{ s.f.})$	$m_{min} = \frac{y_2 - y_1}{X_2 - X_1} = \frac{175\,757.2 - 1\,854.7}{603\,906.2 - 10\,427.3} \approx 0.2930$ $\frac{\Delta m_{min}}{m_{fit}} \times 100\% = \left \frac{m_{min} - m_{fit}}{m_{fit}} \right \times 100\% = \left \frac{0.2930 - 0.3074}{0.3074} \right \times 100\% = 4.7\% \quad (2 \text{ s.f.})$

Table 6 continued: Calculations for Quadratic Linearization and Max/Min Gradient Slopes

Using Table-6, we graph the following:



Graph 2: Linearised Experimental Quadratic-Regression Curve (Graphed using Logger-Pro and Table B1)¹⁰

Graph-2 shows minimal scatter, with $\frac{\Delta m_{max}}{m_{fit}} \times 100\%$ and $\frac{\Delta m_{min}}{m_{fit}} \times 100\%$ varying only 2-5 % (Table-6's Calculation-9 & Calculation-10), further confirming our $E_k \propto (V_0)^2$ hypothesis. Combined with low $\frac{\Delta E_k}{E_k} \times 100\%$ among repeated runs (Table-5), this validates the **veracity** of our findings.

4.3 - Comparison of Theoretical Data and Simulation Data

We cannot use (4) directly to calculate theoretical E_k because it requires **integration** of varying \vec{J} and \vec{B} per timestep, which is only feasible using *Finite-Element-Analysis*. Instead, we simplify by assuming a constant efficiency η , where a fraction of capacitor's initial $E_{Capacitance}$ (1) is converted into armature's E_k :

$$E_{k, \text{theoretical}} = \eta \times \frac{1}{2} \times C \times (V_0)^2 \quad (12)$$

This approach enables us to compare our "ideal" simulated capacitor-bank's efficiency to real-world mass-drivers' efficiencies. By adjusting η in LoggerPro (Vernier Science Education, 2018) so that (12) best fits \bar{E}_k , we determined that $\eta \approx 66.16\%$.

¹⁰ See Appendix-B for Table-B1, listing the linearized values calculated using Table-6.

To visually compare theoretical and processed values, we calculate the following:

Calculation-11: Calculating Theoretical E_k at $\eta \approx 66.16\%$	Example: $E_{k, (\eta=66\%)} = \text{efficiency} \times \frac{1}{2} CV^2$ $= (66.16\%) \times \frac{1}{2} \times C \times (V_0)^2$
Calculation-12: Percentage Difference between \bar{E}_k and $E_{k, (\eta=66\%)}$	Example: $\text{Percentage Difference} = 100\% \times \left \frac{\bar{E}_k - E_{k, (\eta=66\%)}}{E_{k, (\eta=66\%)}} \right $ $\text{Percentage Difference} = 100\% \times \left \frac{181\,683.8 - 186\,075.0}{186\,075.0} \right $ $= 2.4\%_{(1 \text{ d.p.})}$

Table 7: Calculation for Theoretical Values at 750V and Percentage Differences

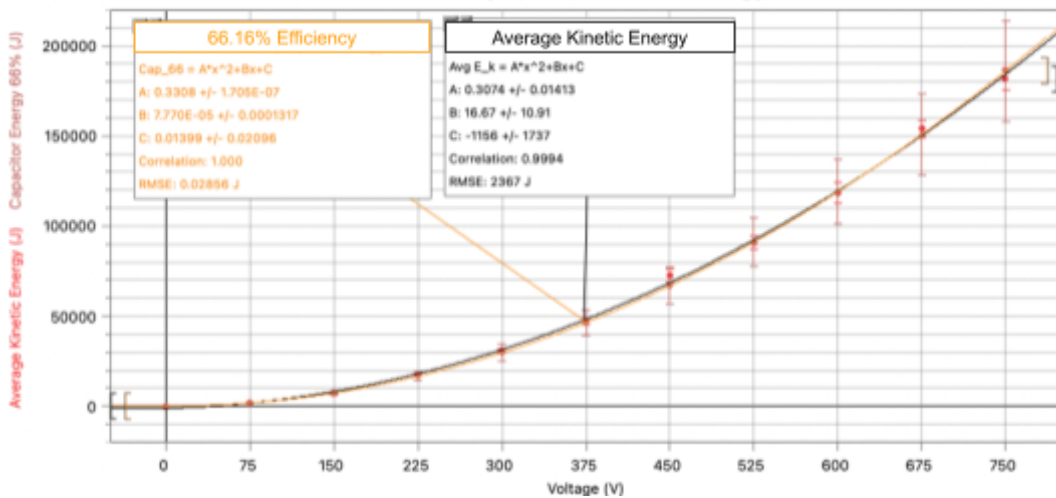
Next, using Table-7:

Initial Voltage of Capacitor Bank V_0 (V)	Average Final Kinetic Energy \bar{E}_k (J)	Final Kinetic Energy given 66.16% mass-driver efficiency $E_{k, (\eta=66\%)}$ (J)	Percentage Difference Between \bar{E}_k and $E_{k, (\eta=66\%)}$
75	1 784.5	1 860.8	4.1 %
150	7 140.5	7 443.0	4.1 %
225	17 447.2	16 746.8	4.2 %
300	30 899.7	29 772.0	3.8 %
375	46 995.2	46 518.8	1.0 %
450	72 500.5	66 987.0	8.2 %
525	90 895.2	91 176.8	0.3 %
600	118 439.8	119 088.0	0.5 %
675	153 963.7	150 720.8	2.2 %
750	181 683.8	186 075.0	2.4 %

Table 8: Voltage-by-voltage comparison between the simulation's final E_k and the 66.16 % theoretical values.

Then, graphing Table-8:

Theoretical 66.16% Efficiency vs. Actual Kinetic Energy of Armature



Graph 3: Comparison of Simulation Results with $\eta = 0.6616$ Theoretical Curve (Graphed using Logger-Pro)

We see Graph-3's $\eta = 0.6616$ curve closely aligns with \bar{E}_k curve, differing by only 1-4 % across most voltages (Table-8). Notably, 450V remains an outlier with ~8 % discrepancy—a deviation likely caused by solver's numerical fluctuations (Vogt et al., 2007). Overall, our simulated mass-driver consistently achieves $\eta = 0.6616$, significantly higher than the literature accepted value of 10 % (Sung, 2008).

4.4 - Comparison with scientific literature

To verify our findings, we consulted established mass-driver literatures. However, existing literatures normally presents “Voltage vs. Velocity v ”, instead of E_k . To compare, we thus converted E_k to v :

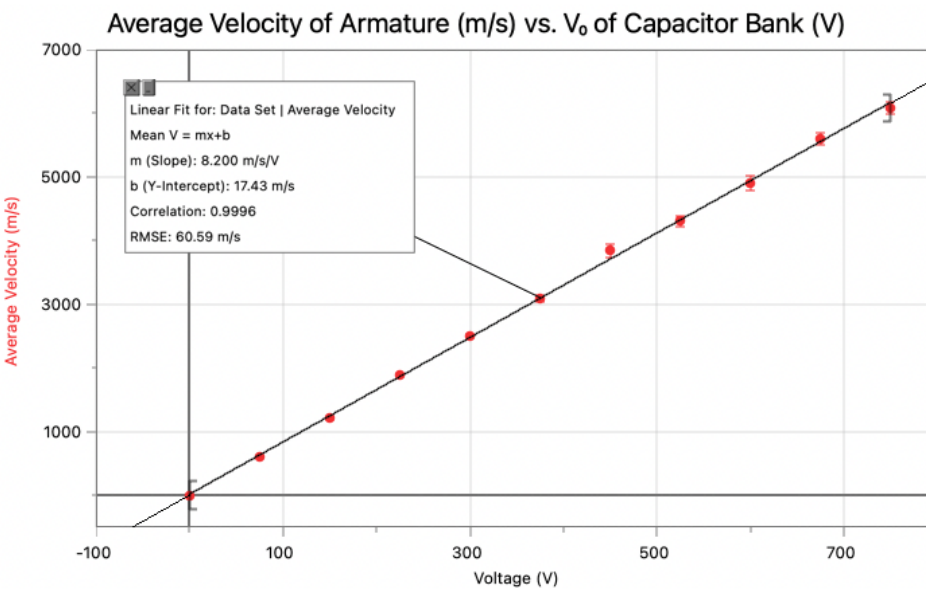
Calculation-13: Average Velocity (\bar{v}) $\bar{v} = \sqrt{\frac{2 \times E_k}{m}}$	Example: $\bar{v} = \sqrt{\frac{2 \times 181\,683.8}{0.009\,83}}$ $\therefore \bar{v} = 6\,079.9 \text{ m/s}_{(1 \text{ d.p.})}$ <i>Note: mass m of armature is 0.009 83 kg</i>
Calculation-14: Absolute Uncertainty ($\Delta\bar{v}$) $\frac{\Delta\bar{v}}{\bar{v}} = \frac{1}{2} \times \frac{\Delta E_k}{E_k}$	Example: $\frac{\Delta\bar{v}}{\bar{v}} = \frac{1}{2} \times \frac{5\,926.6}{181\,683.8}$ $\therefore \Delta\bar{v} = 99.2 \text{ m/s}_{(1 \text{ d.p.})}$

Table 9: Calculation for Converting E_k to v at 750V and Absolute Uncertainties

Using Table-9:

Initial Voltage of Capacitor Bank V_0 (V)	Average Final Kinetic Energy \bar{E}_k (J)	Absolute Uncertainty $\Delta\bar{E}_k$ (J)	Average Final Velocity of Armature \bar{v} (m/s)	Absolute Uncertainty $\Delta\bar{v}$ (m/s)
75	1 784.5	70.2	602.6	11.8
150	7 140.5	261.8	1 205.3	22.1
225	17 447.2	324.5	1 884.1	17.5
300	30 899.7	860.8	2 507.4	34.9
375	46 995.2	1 819.5	3 092.2	59.9
450	72 500.5	3 676.0	3 840.7	97.4
525	90 895.2	3 656.5	4 300.4	86.5
600	118 439.8	5 711.2	4 908.9	118.4
675	153 963.7	4 729.6	5 596.9	86.0
750	181 683.8	5 926.6	6 079.9	99.2

Table 10: Converted v alongside with absolute uncertainty



Graph 4: Armature's Final Velocity vs. Capacitor-bank Voltage (Data from Table 10 and graphed using Logger-pro)

Figures from established literatures (Piekielny et al., 2023, 953-967) (Liu et al., 2014, 32) that we are comparing against:

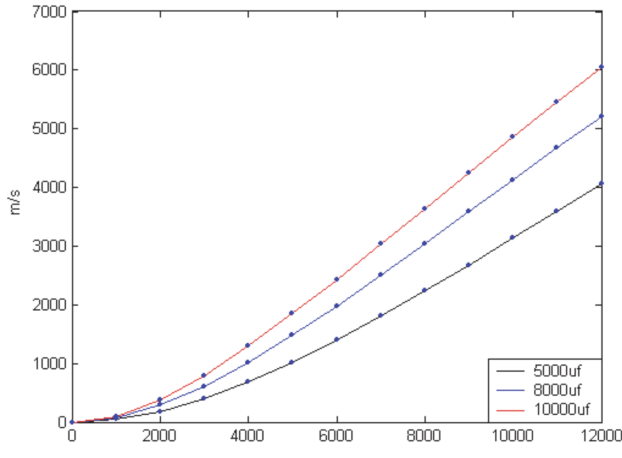


Figure 18: “Relationships between the velocity and the voltage.” by Liu et al.

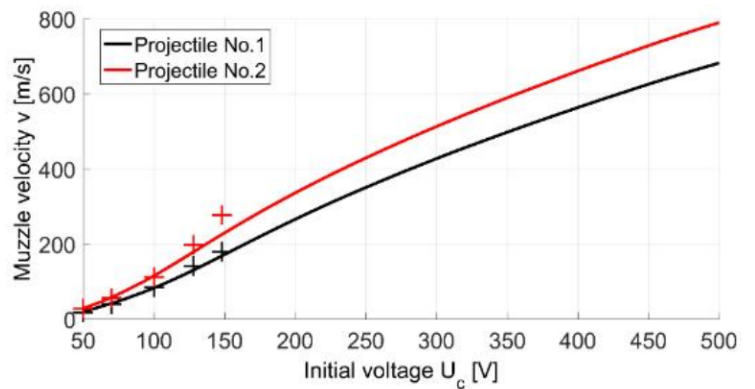


Figure 19: “Initial Velocity vs. Capacitor Initial Voltage” by Piekielny et al.

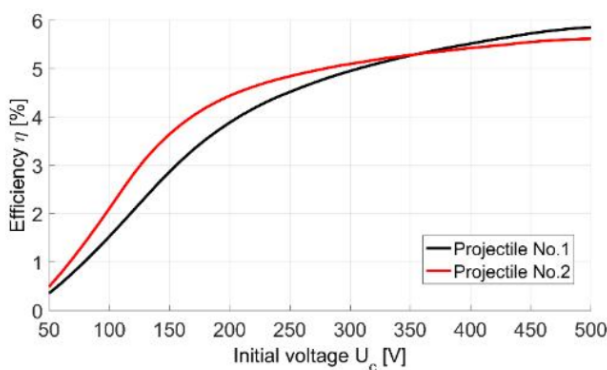


Figure 20: “Efficiency vs. Capacitor Initial Voltage” by Piekielny et al.

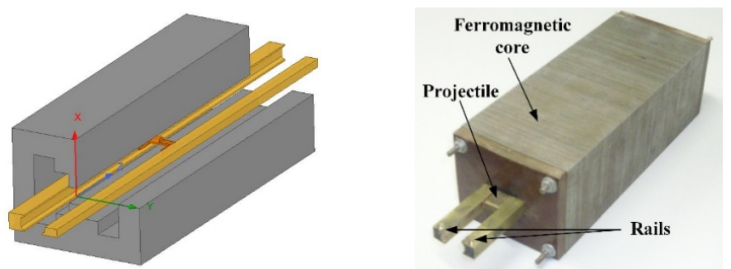


Figure 21: “Iron-core mass-driver with permanent magnet support” by Piekielny et al.

4.4.1 - Comparison to Existing Literature - Our Empirical Trend

Our finding that $V_0 \propto (E_k)^2$ (and hence $V_0 \propto v$ since $E_k = \frac{1}{2}mv^2$) aligns with Liu’s simulation (Liu et al., 2014, 29-34), which, like our procedure, assumes an ideal RLC circuit omitting drag and friction. Liu reports a **near-linear voltage-velocity relationship** (Figure-18), mirroring our empirical findings (Graph-4).

In contrast, Piekielny’s practical mass-driver (Piekielny et al., 2023, 953-967) uses an augmented design with ferromagnetic cores (Figure-21). Piekielny’s reports a **non-linear voltage-velocity curve** (Figure-19)—especially above 200V—likely due to real-world losses like air-resistance that become significant at high speeds. Piekielny’s **non-linearity**, which deviates from our and Liu’s results, illustrates how real-world factors reduce velocity gains at higher V_0 .

4.4.2 - Comparison to Existing Literature - Our Mass-Driver’s Efficiency

Large-scale mass-drivers normally achieve 10–50 % efficiency (Sung, 2008), while amateur-builds often manage < 1%. Indeed, our practical mass-driver build reached ~3% efficiency (Appendix-A), while Piekielny’s attains 1–6% (Figure-20), leveling off at higher V_0 due to friction, arcing and air-resistance.

In contrast, our LS-DYNA mass-driver achieves ~66% efficiency (Graph-3) and Liu’s reports 45%—both much higher than practical builds. This discrepancy highlights the overestimation of E_k in idealized simulations that omit real-world energy losses. Thus, if we investigated using a practical mass-driver, we likely wouldn’t observe a neat near-linear trend (Graph-4), but rather a nonlinear curve which levels off at higher V_0 , along with lower efficiency—similar to Piekielny’s findings (Figure-19).

5 Conclusion

Our data clearly confirms that, under ideal LS-DYNA conditions, **increasing the Capacitor-bank's V_0 from 75V to 750V yields a quadratic increase in the armature's E_k** . Our quadratic-fit's high $R^2 = 0.9988$, alongside with our error-bars' consistently small percentage uncertainty between 1–5 %, with $\frac{\Delta m_{max}}{m_{fit}} \times 100\%$ and $\frac{\Delta m_{min}}{m_{fit}} \times 100\%$ varying only 2–5 %, reinforces our empirical finding's **veracity**.

Our demonstrations of $V_0 \propto (E_k)^2$ relationship is valuable, as it shows, in the absence of real-world factors like gravity and air-drag, this relationship naturally holds for RC-circuit mass-drivers. However, practical mass-drivers rarely use high-capacitance and high-voltage capacitor-banks, relying instead on **pulsed-power supplies** (Lan, 2012) (First Light Fusion, n.d.). This reduces our findings applicability—especially for designing *inertial-confinement-fusion* reactors.

Extrapolating our quadratic-fit beyond 750V is unlikely to be useful, because our $9.83g$ armature already reaches **Mach 17.5** at 750V—exceeding typically *inertial-confinement-fusion* velocity requirements (Wang, 2024), thus diminishing extrapolation's utility.

However, as discussed in Section-4.4, **real-world factors** would likely invalidate our neat $V_0 \propto (E_k)^2$ relationship. As demonstrated by Piekielny's results, **non-linear** trend emerges once practical losses are introduced, further limiting our finding's direct applicability.

6 Evaluation

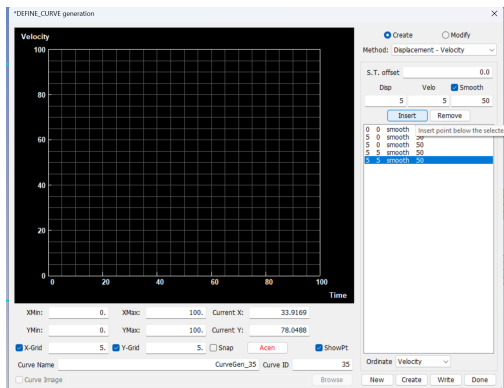


Figure 22: LS-DYNA `define_curve` Window
(DYNAmore GmbH, n.d.)

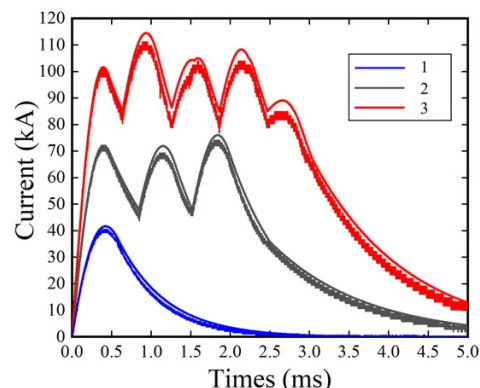


Figure 23: Pulsed-Power Supply Discharge Current Waveform (Cao et al., 2022)

6.1 - Design Error

Design Error	Explanation	Impact	Proposed Solutions
Incrementation of 75V	We used 10 increments between 75V–750V, which totalled ~23 hours of computation; smaller increments would've exceeded our computational budget.	Subtle non-linearities between 75V intervals likely missed. Which fewer intermediate data points reduce interpolation certainty.	Use 25V increments if additional computational resources allow, improving our finding's resolution and generalizability.

Table 11: Design Error Evaluation Table

6.2 - Systematic Error

Systematic Error	Explanation	Impact	Proposed Solutions
Translational Constraints applied in FEA	In FEA, translational constraints are normally required to simplify calculations (Watson et al., 2017). For this investigation, translational constraints prevent the armature from penetrating the rails (causes simulation failure), but eliminate lateral motion and frictional contact, thus inflating E_k .	<ul style="list-style-type: none"> Direction: Overestimates E_k. Magnitude: Large at high velocity, as $F_{friction}$ and real-world losses increase with velocity. 	<ul style="list-style-type: none"> - Enable friction/contact models in LS-DYNA's structural solver to reflect real-world rail-armature interactions, improving accuracy and applicability. - Outcome: More realistic results that can be generalized better to practical mass-driver designs.
No Atmosphere, Gravity and Plasma Arcing	Our simulation ignores air-drag, gravity, and plasma-arcing. This assumption is valid for ICF reactors—often housed in vacuum chambers (First Light Fusion, n.d.)—but not for Earth-based mass-drivers like China's proposal (SCMP, 2024), where air-drag at high speed significantly reduces acceleration. In both systems, plasma-arcs (at higher V_0) cause significant energy losses and rail erosion (Vricella et al., 2017), like my practical mass-driver build (Figure-26).	<ul style="list-style-type: none"> Trend Impact: Real-world data likely deviates from $V_0 \propto (E_k)^2$ trend because real-world losses increase with velocity. Causing non-linear relationships like Figure-19's, reducing our finding's applicability. 	<ul style="list-style-type: none"> - Earth-based Systems: Enable plasma-arcing, air-drag and gravity in LS-DYNA to simulate real-world factors. - ICF Reactors: Incorporate plasma-arcing and gravity to reflect real-world rail erosion and energy dissipation. - Outcome: More realistic simulations enhance our finding's <i>applicability</i>, aligning more closely with actual operating conditions and thereby improving <i>generalizability</i>.
Mesh Quality & Timestep	Coarser meshes and larger timesteps reduces simulation accuracy. Denser meshes and smaller timesteps increases accuracy but also computational cost.	<ul style="list-style-type: none"> Direction: \pm variation in E_k (no consistent bias) Magnitude: < 1% difference, but larger if mesh too coarse. (Waindok, 2017, 153) Trend Impact: Minor effect; lowers precision but overall quadratic finding likely remains. 	<ul style="list-style-type: none"> - Refine mesh and reduce timestep to capture details, improving finding's <i>accuracy</i> and <i>reliability</i>.
Oversized 1.0F Capacitor Bank	Practical mass-drivers typically use pulsed-power supplies over large-capacitance capacitor-banks (Sung, 2008). As pulsed-power normally delivers short, high current bursts more cost-effectively. Hence, this investigation's use of RC-circuit reduces our finding's applicability.	<ul style="list-style-type: none"> Direction: Overestimates E_k at higher V_0. Magnitude: Likely significant because real pulses are shorter than RC-circuits, making performance appear better than real-world pulsed-power setups. Trend Impact: RC-circuit preserves $V_0 \propto (E_k)^2$ trend but reduces finding's <i>applicability</i> for real-world mass-driver. 	<ul style="list-style-type: none"> - Use DEFINE_CURVE keycard (Figure-22) to replicate pulsed-power discharge characteristics (Figure-23). Then, apply this curve as mass-driver's power input, improving our result's <i>applicability</i>.

Table 12: Systematic Error Evaluation Table

6.3 - Random Error

Random Error	Explanation	Impact	Proposed Solutions
Stochastic Solver Variation	Even under identical conditions, LS-DYNA's variability produces minor run-to-run scatter due to floating-point round-off, and timestep approximations (Vogt et al., 2007).	<ul style="list-style-type: none"> Direction: \pm variation in E_k (no consistent bias) Magnitude: Combined variation of 1-5 % (Table-5) for E_k. 	<ul style="list-style-type: none"> More Repeats: Already done 7 per voltage, but additional repeats boost reliability. - Reduce timestep if computational resources allow, improving precision of findings by minimizing approximation errors.
Mesh Discretization Uncertainty	The exemplar's default mesh may overlook fine-scale field variations, causing local misrepresentation of \vec{J} and \vec{B} , causing random E_k fluctuations (Schwer, 2008).	<ul style="list-style-type: none"> Trend Impact: Minimal effect on $V_0 \propto (E_k)^2$ trend, but lowers repeatability and precision. 	<ul style="list-style-type: none"> - Use finer mesh if computational resources allow, improving precision of findings. - Convergence Studies: Checking multiple mesh densities help confirm stable and repeatable solutions (Schwer, 2008).

Table 13: Random Error Evaluation Table

6.4 - Future Extension

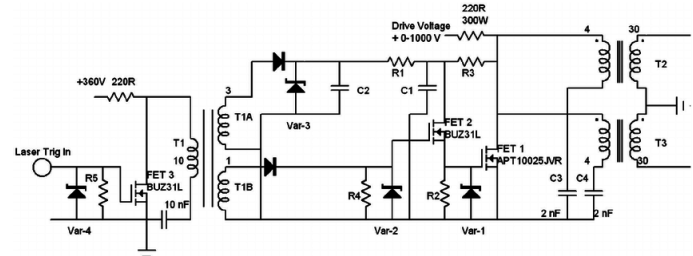


Figure 24: Pulsed-power Supply Circuit Diagram
(Welsh et al., 2007)

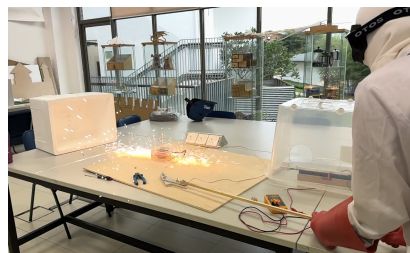


Figure 25: Student's Real-world Mass-Driver Build (more detail in Appendix A)



Figure 26: Student's Mass-Driver Plasma-Arcing during Testing Trials

Build a practical mass-driver (Figure-25) to validate whether $V_0 \propto (E_k)^2$ trend holds when real-life factors like friction and plasma-arching (Figure-26) are at play. Any discrepancies with LS-DYNA will be used to recalibrate model parameters, boosting our findings' applicability. Optionally, use pulsed-power supply (Figure-24) to more rigorously emulate real-world conditions.

References

- Ansys Inc. (n.d.). *Ansys LS-DYNA Student Version*. Ansys. Retrieved February 25, 2025, from
<https://www.ansys.com/academic/students/ansys-ls-dyna-student>
- Ansys Inc. (n.d.). *LSDYNA Download / Install Overview*. LS-DYNA. Retrieved May 13, 2024, from
<https://lsdyna.ansys.com/download-install-overview/>
- Ansys Inc. (n.d.). *Railgun — Welcome to LS-DYNA Examples*. LS-DYNA Examples. Retrieved May 13, 2024, from
https://www.dynaexamples.com/em/eddycurr/em_railgun
- Ansys Inc. (n.d.). *Welcome to the LS-DYNA Product Space*. LSDYNA Home. Retrieved February 25, 2025, from
<https://lsdyna.ansys.com/>
- Ansys Inc. (2024, August 1). *LS Run 2024R2.xlsx*. Ansys. Retrieved February 26, 2025, from
<https://www.ansys.com/content/dam/web/vpats/ls-run-2024r2.pdf>
- Ansys Inc. (2024, December 18). *LS-DYNA Manual*. LS-DYNA Materials Manual. Retrieved February 25, 2025, from
https://ftp.lstc.com/anonymous/outgoing/web/ls-dyna_manuals/DRAFT/DRAFT_Vol_II.pdf
- Beach, F. C. (1996, June). Design and Construction of a One Meter Electromagnetic Railgun. Retrieved May 13, 2024, from <https://archive.org/details/designconstructi00beac>
- Blender.org. (n.d.). blender.org - Home of the Blender project - Free and Open 3D Creation Software. Retrieved May 13, 2024, from <https://www.blender.org/>
- Boz, Z., Erdogdu, F., & Tutar, M. (2014, February). Effects of mesh refinement, time step size and numerical scheme on the computational modeling of temperature evolution during natural-convection heating. *Journal of Food Engineering*, 123, 8-16. <https://doi.org/10.1016/j.jfoodeng.2013.09.008>
- Çaldichoury, I., & L'Eplattenier, P. (2012, July). Simulation of a Railgun: A contribution to the validation of the Electromagnetism module in LS-DYNA® v980. *LS-DYNA User Conference*, 12.
https://www.researchgate.net/publication/337448381_Simulation_of_a_Railgun_A_contribution_to_the_validation_of_the_Electromagnetism_module_in_LS-DYNAR_v980
- Çaldichoury, I., & L'Eplattenier, P. (2012, July). Simulation of a Railgun: A contribution to the validation of the Electromagnetism module in LS-DYNA® v980. *LS-DYNA User Conference*, 12.
https://www.researchgate.net/publication/337448381_Simulation_of_a_Railgun_A_contribution_to_the_validation_of_the_Electromagnetism_module_in_LS-DYNAR_v980
- Cao, G., Xiang, H., Qiao, Z., Liang, C., Yuan, X., Wang, J., & Lei, B. (2022, July 11). Utilization Optimization of Capacitive Pulsed Power Supply in Railgun. *Energies* 2022, 15(5051). <https://doi.org/10.3390/en15145051>

Codefinity. (n.d.). *Learn 3-Sigma Rule | Statistical Methods in Anomaly Detection*. Codefinity. Retrieved February 26, 2025, from
<https://codefinity.com/courses/v2/165dbadd-b48e-4a7f-8b0d-1b8477c22a1d/047e166d-bc62-4bd1-8114-f0771ef62d83/a087d692-2177-4251-ac77-9466243454e4>

David, L. (2024, June 24). *Could we launch resources from the moon with electromagnetic railguns?* Space.com.

Retrieved January 1, 2025, from <https://www.space.com/electromagnetic-launch-moon-mass-drive>

Ding, M. (2024, March 4). *What is the price of Ansys?* Resources. Retrieved February 25, 2025, from
<https://blog.ozeninc.com/industry-applications/ansys-pricing>

DYNAmore GmbH. (n.d.). *Double precision*. LS-DYNA Support. Retrieved February 25, 2025, from
<https://www.dynasupport.com/howtos/general/double-precision>

DYNAmore GmbH. (n.d.). *LS-DYNA Manuals — Welcome to the LS-DYNA support site*. LS-DYNA support. Retrieved February 26, 2025, from <https://www.dynasupport.com/manuals/ls-dyna-manuals>

DYNAmore GmbH. (n.d.). *LS-PREPOST*. LS-DYNA Support. Retrieved February 26, 2025, from
<https://www.dynamore.de/en/products/pre-and-postprocessors/prepost>

First Light Fusion. (n.d.). *Largest Pulsed Power Facility in Europe | M3 Machine*. First Light Fusion. Retrieved May 13, 2024, from <https://firstlightfusion.com/technology/m3>

HPCwire. (2024). *Renewable Power Unlock New Efficiencies for High-Performance Computing*. HPCwire. Retrieved February 26, 2025, from

<https://www.hpcwire.com/renewable-power-unlock-new-efficiencies-for-high-performance-computing/>

IAEA. (n.d.). *Fusion - Frequently asked questions | IAEA*. International Atomic Energy Agency. Retrieved February 26, 2025, from <https://www.iaea.org/topics/energy/fusion/faqs>

Lan, J. (2012, May 19). Design and optimization of the pulsed power supply system used for electromagnetic railgun.
2012 16th International Symposium on Electromagnetic Launch Technology.

<https://doi.org/10.1109/EML.2012.6325159>

Liu, C. (n.d.). *The Three-Body Problem (Remembrance of Earth's Past, #1....* Goodreads. Retrieved February 25, 2025, from <https://www.goodreads.com/book/show/20518872-the-three-body-problem>

Liu, J. M., BAO, Z., WANG, Z., & LIU, F. (2014, February 28). A Measuring Method About the Bullet Velocity in Electromagnetic Rail Gun. *Sensors & Transducers*, 165(2), 29-34. Retrieved May 13, 2024, from
https://www.researchgate.net/publication/282300092_A_Measuring_Method_About_the_Bullet_Velocity_in_Electromagnetic_Rail_Gun

- Los Alamos Scientific Laboratory, T., P. A., & United States Department of Energy Office of Policy and International Affairs. (1979, July 10-12). Proceedings of the Impact Fusion Workshop. 1-471.
- <https://onlinebooks.library.upenn.edu/webbin/book/lookupid?key=ha102569000>
- Lou, Y., Wan, G., Jin, Y., Tang, B., & Li, B. (2016, May). Research on Energy Loss Distribution of an Augmented Railgun. *IEEE Transactions on Plasma Science*, 44(5), 857-861. <https://doi.org/10.1109/TPS.2016.2542217>
- McFarland, J., & McNab, I.R. (2003, January). A long-range naval railgun. *IEEE Transactions on Magnetics*, 39(1), 289-294. <http://dx.doi.org/10.1109/TMAG.2002.805924>
- OpenAI LLC. (n.d.). *ChatGPT O1 Pro*. ChatGPT. Retrieved February 26, 2025, from <https://chatgpt.com/?model=o1-pro>
- Student comment:** I have used ChatGPT Pro (O1 pro model) to assist me in grammatical check, brainstorming and researching sources.
- Example chat: <https://chatgpt.com/share/67be0014-f0a0-8003-9091-ed231485d645>
- Piekielny, P., Tomczuk, B., & Waindok, A. (2023, July 27). Characteristics simulations of the electrodynamic railgun different constructions and their measurement verification. *ARCHIVES OF ELECTRICAL ENGINEERING*, 72, 951-969. <https://doi.org/10.24425/aee.2023.147420>
- Saballa, J. (2021, July 8). *US Navy Halts Development of Electromagnetic Railgun*. The Defense Post. Retrieved February 26, 2025, from <https://thedefensepost.com/2021/07/08/us-navy-railgun/>
- Sandia National Laboratories. (n.d.). *Inertial Confinement Fusion – Pulsed-Power Science and Technology*. Sandia National Laboratories. Retrieved February 25, 2025, from <https://www.sandia.gov/pulsed-power/inertial-confinement/>
- Schwer, L. E. (2008). IS YOUR MESH REFINED ENOUGH? Estimating Discretization Error using GCI. 7. *LS-DYNA Anwenderforum 2008*, 1-10. <https://www.dynamore.de/de/download/papers/forum08/dokumente/I-I-03.pdf>
- ScienceDirect. (2019). Lorentz Force. Retrieved January 6, 2025, from <https://www.sciencedirect.com/topics/physics-and-astronomy/lorentz-force>
- SCMP. (2024, March 14). *China plans to build a giant rail gun to launch hypersonic planes into space*. South China Morning Post. Retrieved January 8, 2025, from <https://www.scmp.com/news/china/science/article/3255351/nasas-dream-comes-true-china-plans-build-giant-rail-gun-launch-hypersonic-planes-space>
- Stanford University & Thavapatikom, G. (2012, December 12). *Railgun Payload Launch*. Stanford. Retrieved January 3, 2025, from <http://large.stanford.edu/courses/2012/ph240/thavapatikom2/>

- Sung, V. (2008, Summer). Lumped Parameter Modeling of the Ideal Railgun: Examining Maximum Electromechanical Energy Conversion Efficiency. 1-16. <https://www.rose-hulman.edu/~wheeler/PDF/publications.PDF>
- Universiti Malaya. (n.d.). *Personal Carbon Footprint Calculator*. Malaysian Green Technology And Climate Change Corporation. Retrieved January 9, 2025, from <https://www.mgtc.gov.my/lcos-personal-calculator/>
- Vernier Science Education. (2018, March 18). *How do you calculate linear fits in Logger Pro?* Vernier.com. Retrieved January 8, 2025, from <https://www.vernier.com/tl/1869>
- Vogt, D., Hartnack, R., Olbert, M., & Schlattmann, J. (2007). Uncertainty Assessment with Stochastic Simulation in Aircraft Cabin Development. *6th European LS-DYNA Users' Conference*, 6, 1-12.
<https://lsdyna.ansys.com/wp-content/uploads/attachments/uncertainty-assessment-with-stochastic-simulation.pdf>
- Vricella, A., Delfini, A., Pacciani, A., Pastore, R., Micheli, D., Rubini, G., Marchetti, M., & Santoni, F. (2017). A new advanced railgun system for debris impact study. *Procedia Structural Integrity*, 3, 545-552.
<https://doi.org/10.1016/j.prostr.2017.04.044>
- Waindok, A. (2017, February). Transient Analysis of a Railgun with Iron Core. *PRZEGŁĄD ELEKTROTECHNICZNY*, 152-155. <http://dx.doi.org/10.15199/48.2017.02.33>
- Wang, B. (2024, April 15). *First Light Fusion Makes Progress Towards an Economical Working Fusion Reactor*. NextBigFuture.com. Retrieved February 26, 2025, from <https://www.nextbigfuture.com/2024/04/first-light-fusion-makes-progress-towards-an-economical-working-fusion-reactor.html>
- Warnock, D. S. (2003, September). Design and optimization of a 600-KJ railgun power. 85.
<https://hdl.handle.net/10945/6254>
- Watson, P. J., Dostanpor, A., Fagan, M. J., & Dobson, C. A. (2017, May). The effect of boundary constraints on finite element modelling of the human pelvis. *Medical Engineering & Physics*, 43, 48-57.
<https://doi.org/10.1016/j.medengphy.2017.02.001>
- Welsh, G. H., Turton, D. A., Jones, D. R., & Jaroszynski, D. A. (2007, May). 200 ns pulse high-voltage supply for terahertz field emission. *Review of Scientific Instruments*, 78(4). <http://dx.doi.org/10.1063/1.2724769>

Appendix A

We used LS-DYNA in this paper to explore the research question because the time, fabrication skills, and resources needed for a physical build were not feasible within our timeframe. Nonetheless, to further my engineering skills and deepen my understanding of fusion technology, I constructed a practical mass driver on my own. Below, I outline the procedures, safety considerations, and qualitative observations gathered during testing.

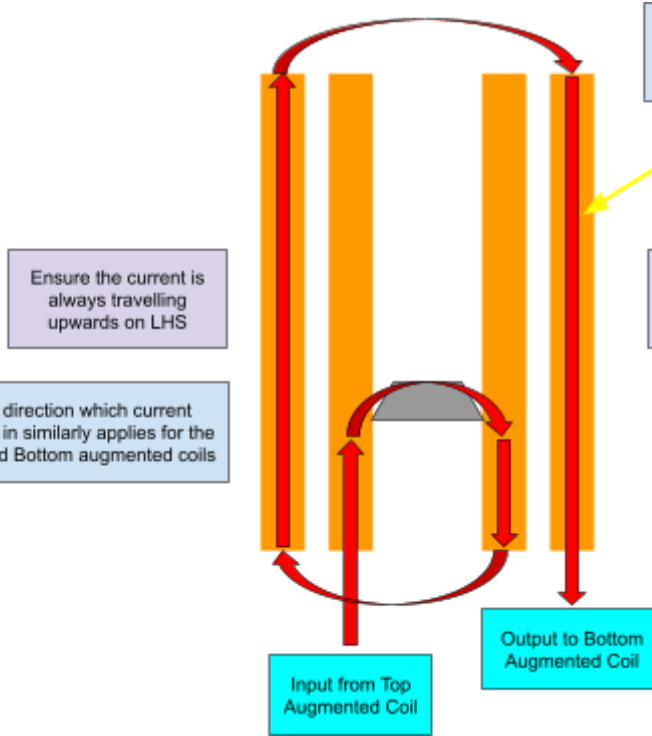


Figure A1: Current flow direction guide in augmented rails

11

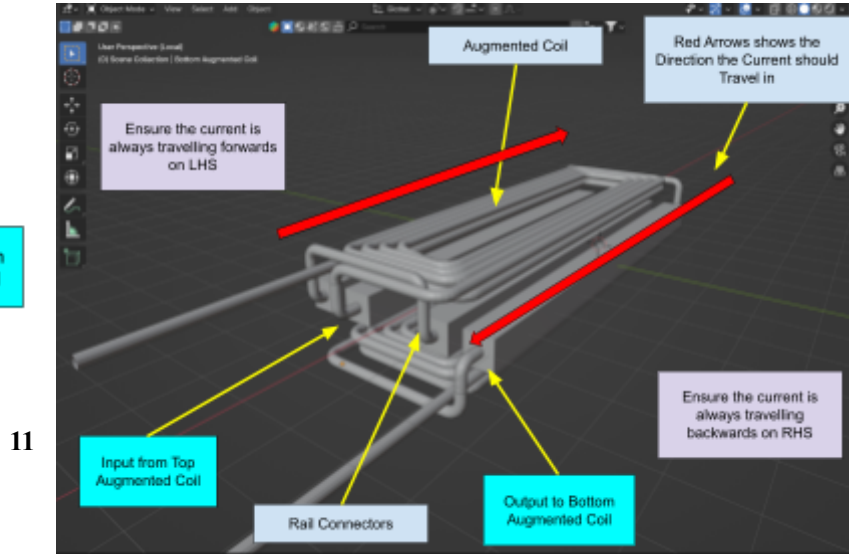


Figure A2: LS-Dyna Exemplar Mass-driver Geometry

Figure A3: 3D Model Labelled with Desired Current Flow Directions (Designed in Blender)

In contrast to the simpler geometry used in LS-DYNA's exemplar (see Figure A2) (Ansys Inc., n.d.), my practical design incorporates **augmented rails** and **coils** for higher efficiency.

Augmented rails channels more current $I(t)$ close to the armature, which increases both \vec{B} and \vec{J} near the armature. According to (2), this increases $\vec{F}_{Lorentz}$ for the same power input. Hence, improved efficiency. To implement augmentation successfully, the current on the left-hand side of the armature must always flow forward, and vice versa (see Figure-A1 & Figure-A3). Otherwise, the augmented rail's $\vec{F}_{Lorentz}$ will cancel out the main rail's $\vec{F}_{Lorentz}$, reducing the overall efficiency of the mass-driver.

This also applies to augmented coils (Figure A3), where ensuring proper current flow in designated directions is crucial for maximizing mass-driver efficiency.

¹¹ Augmentation design inspired by (Beach, 1996, 22)

Procedure (Practical Setup)

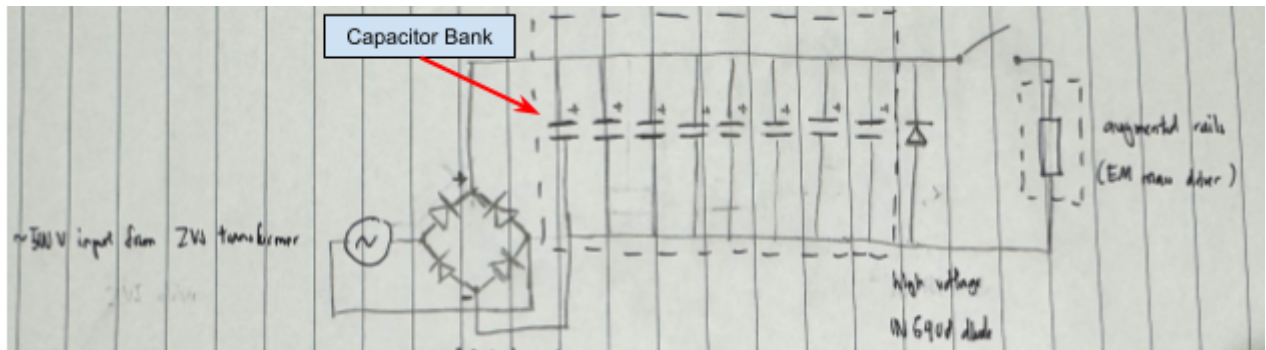


Figure A4: Circuit Diagram demonstrating mass-driver layout

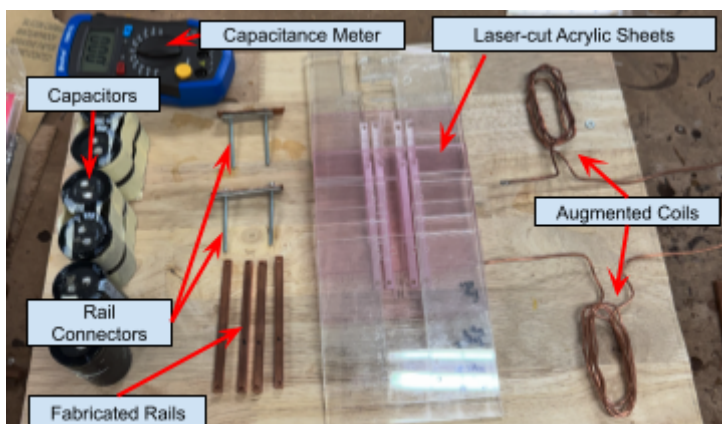


Figure A5: Fabricated Components

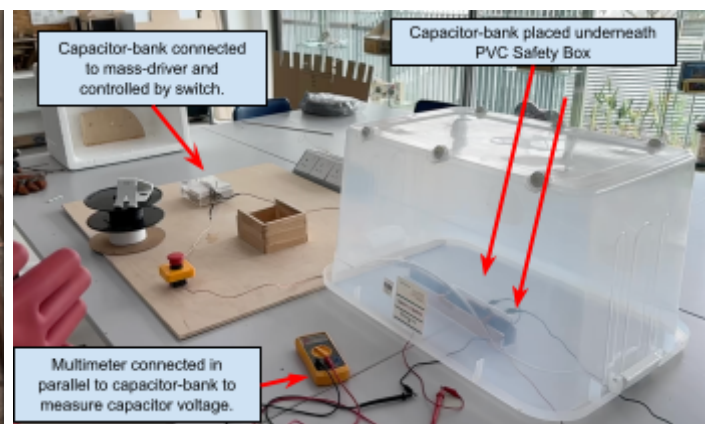


Figure A6: Mass-Driver Assembled Layout

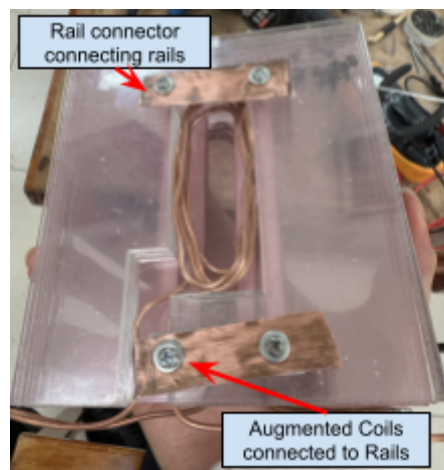


Figure A7: Close-up of Acrylic Housing



Figure A8: Capacitor-Bank with pins soldered to copper strip.

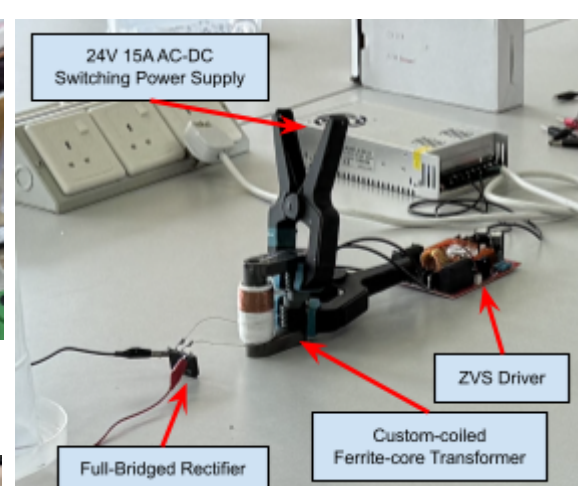


Figure A9: ZVS Charging Setup

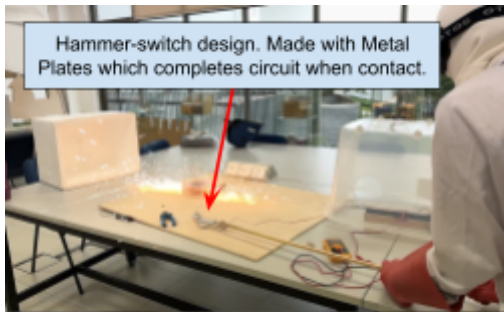


Figure A10: Hammer-switch

1. **Design**
 - a. **CAD Modeling:** Use any preferred CAD software (e.g., Blender (*Blender.org*, n.d.)) to design an augmented mass-driver (Figure A3).
 - b. **Housing Layout:** Incorporate an acrylic housing (Figure A7) that holds rail connectors, rails, and augmented coils. The dimensions are flexible, as long as the design enable current flow direction align with the intended current path (Figure A1 & Figure A3) to optimize efficiency.
2. **Cut and Coil (Figure A5)**
 - o **Rails & Connectors:** Based on CAD design, fabricate 6 mm copper rails to the required lengths and drill holes at both ends for rail connectors. Cut copper sheets for rail connectors (thickness is flexible).
 - o **Acrylic Components:** Laser-cut 5 mm acrylic sheets based on CAD-generated SVG files. These sheets will hold the rails, rail connectors, and augmented coils.
 - o **Augmented Coil:** Wind 2 mm diameter copper wire into augmented coils according to the CAD specifications (Figure A3).
2. **Assembly**
 - o **Mounting:** Attach rails, rail connectors, and augmented coils to the laser-cut acrylic using M3 screws (Figure A7).
 - o **Verify Connections:** Confirm the current flow follows the desired path (Figures A1 & A3).
 - o **Capacitor Bank:** Solder capacitors' pins to a low-resistance copper strip (Figures A8 & A19). Low resistance is crucial to minimize $I(t)$ loss per Equations (2) and (3).
 - o **Safety Enclosure:** Place the capacitor-bank under a safety shield to guard against potential capacitor failure. (Figure A6)
3. **Configure Charging**
 - o Attach the ZVS transformer and associated wiring with switching power supply (Figure A9) so the capacitor bank can be charged safely (see Figure A4 & A6). Coil the transformer such that the output voltage prevents overcharging risks.
4. **Complete the Circuit**
 - o **Wiring:** Connect all components according to the circuit diagram (Figure A4).
 - o **Polarity Check:** Confirm capacitor-bank polarity. **Important:** Reversed polarity can cause capacitor explosions.
 - o **Short-Circuit Inspection:** Verify no unintended short circuits before powering on.
5. **Operate the System**
 - o **Charging:** Switch on the power supply to charge the capacitor bank (stepped up by the ZVS transformer). Monitor voltage with a parallel multimeter (Figure A6).
 - o **Activation:** Once the desired voltage is reached, close the high-power switch (Figures A6 & A10). The resulting Lorentz force accelerates the armature along the rails.

(Continue to next page)

Equipments required:

Capacitor Bank	8× 400 V, (1000 ± 10%) μ F Aluminium-electrolytic capacitors		1N5408 Diode			
Augmented Coil	2 mm diameter copper wire (2 m length)					
Rails	6 mm copper rods					
Armature	Copper staple					
Supporting Structure	5 mm acrylic sheets (laser cutted)	M3 60mm Screws	Copper Sheets			
Capacitor-Bank Charging System	ZVS driver	Ferrite Transformer Core	1000V 30A Full Bridge Rectifier	24V 15A Switching Power Supply		
Measuring Equipment	Multimeter (\pm (2% + 2.0V))		Capacitance Meter \pm (4% + 20 μ F)			
	Digital Caliper (\pm 0.00001m)					
Additional Equipment	High-powered Switch					
Safety	High-voltage Gloves	Rubber Boots	Face Shield	Safety Screen		
	Noise-Cancelling Headphones					

Table A1: Apparatus required (Specification flexible, may vary slightly)

Safety and Environmental Considerations

Safety	<p>High-voltage capacitors pose a serious shock hazard, so teacher supervision is required at all times. PPE—face shield, high-voltage gloves, rubber boots, and noise-cancelling headphones (ear-protection)—is mandatory to protect against both the intense noise of capacitor discharges and the danger posed by high voltage.</p> <p>To mitigate the risk of capacitor explosion during the charging process, the capacitor-bank is placed under a sturdy plastic enclosure.</p> <p>Even when the multimeter reads 0 V, in my experience, some capacitors from the capacitor-bank tend to retain residual voltages of 100 V or more. Consequently, the safety protocol is, each unit in the capacitor bank is measured individually frequently, and any residual charge is discharged using insulated pliers before handling.</p> <p>Finally, when activating the mass-driver, the armature is directed towards a protective box, to prevent risk of injury from fast moving armature.</p>
Environmental Impact	<p>Construction used mostly salvaged scrap acrylic from my school's workshop, minimizing waste and resource usage.</p>

Table A2: Practical Setup - Safety and Environmental Considerations

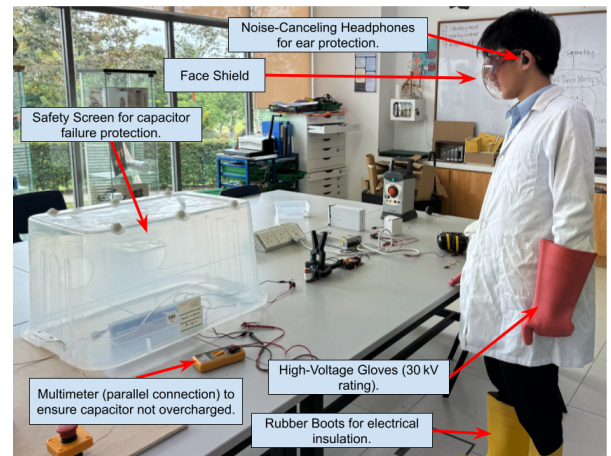


Figure A11: Safety Precautions

Qualitative Observations (Practicals)

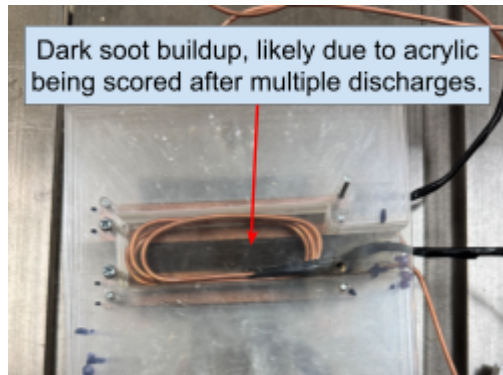


Figure A12: Mass-Driver Soot-build

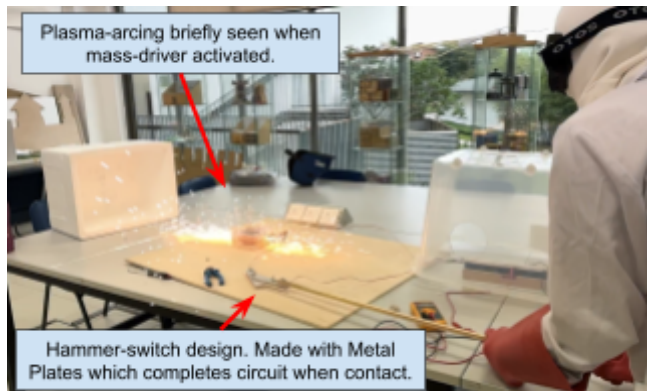


Figure A13: Plasma-Arcing

When our **practical mass-driver** (Figure A13) is activated after being charged, **plasma-arcing** is visibly seen, accompanied by a **loud bang**—indicating that a significant portion of the capacitor-bank $E_{Capacitance}$ is lost as **heat** and **sound**. In particular, at 400V, **slow-motion footage** shows the armature reaching **93 m/s**, yielding an **approximate 3% efficiency**. This stands in contrast to the **66.16%** efficiency observed in our LS-DYNA simulation and the **10 %** efficiency typical of many practical mass-drivers (Sung, 2008).¹²

After more than ten test trials, **soot** buildup became evident (Figure A12). This is potentially due to **plasma generation** burning the acrylic support structure, demonstrating how real-world mass-drivers suffer from erosion and byproducts.

Appendix B

Initial Voltage of Capacitor Bank V_0 (V)	Linearised Voltage $X = (V_0 + 27.114)^2$ (V ²)	Average Final Kinetic Energy \bar{E}_k (J)	Absolute Uncertainty $\Delta\bar{E}_k$ (J)
75	10427.3	1 784.5	70.2
150	31369.4	7 140.5	261.8
225	63561.5	17 447.2	324.5
300	107003.6	30 899.7	860.8
375	161695.7	46 995.2	1 819.5
450	227637.8	72 500.5	3 676.0
525	304829.9	90 895.2	3 656.5
600	393272.0	118 439.8	5 711.2
675	492964.1	153 963.7	4 729.6
750	603906.2	181 683.8	5 926.6

Table B1: Linearised Values alongside with Absolute Uncertainty (Calculated using Table 6)

¹² Acknowledged in Section-6. These losses likely stem from real-world factors such as friction, rail erosion, and voltage arcing—none of which are fully captured by the idealized simulation.

Appendix C

Appendix C.1 – LS-DYNA Part Data File

If interested, see the original manual from LS-DYNA (DYNAmore GmbH, n.d.). Below is an exemplar “[EM_PART_DATA_0001.dat](#)” file dedicated to the armature. LS-DYNA records all armature related statistics at each timestep when “[EM_DATABASE_PART](#)” is activated.

We have omitted most columns and shown only those relevant to this investigation:

- $F_{Lorentz}$ along the x-axis
- $F_{Lorentz}$ along the y-axis
- $F_{Lorentz}$ along the z-axis
- The armature’s Joule Heating Energy
- The armature’s Magnetic Energy
- The armature’s Kinetic Energy

Below contains the raw part data for $V_0 = 150V$ (Trial 1). The final E_k is highlighted. Since the LS-DYNA exemplar file uses mm/g/mC/s as base units, Kinetic Energy is recorded in nJ. Hence, a final $E_k = 0.6942 \times 10^{13} \text{ nJ} = 6942.3 \text{ J}$.

EM Mass-Driver example

```
ls-dyna smp d R13 R13.1.1_27_8731a0 date 07/28/2023
```

EM Part data

time	LorFor-x	LorFor-y	LorFor-z	JHEnergy	MagEnergy	KinEnergy
0.1000000E-04	0.8097291E+08	0.1475420E+09	0.2891148E+08	0.1125962E+15	0.3155254E+09	0.0000000E+00
0.2000000E-04	0.2787652E+09	0.5099106E+09	0.1095302E+09	0.3283572E+15	0.1464411E+10	0.8210165E+04
0.3000000E-04	0.5458694E+09	0.9264092E+09	0.2133986E+09	0.5635714E+15	0.3343740E+10	0.2453188E+06
0.4000000E-04	0.8803732E+09	0.1212000E+10	0.2586244E+09	0.7398523E+15	0.5541451E+10	0.2017114E+07
0.5000000E-04	0.1246887E+10	0.1306747E+10	0.2909561E+09	0.9096861E+15	0.7991970E+10	0.9166938E+07
0.6000000E-04	0.1639609E+10	0.1258723E+10	0.3143921E+09	0.1058298E+16	0.1058749E+11	0.2933269E+08
0.7000000E-04	0.2125820E+10	0.9444288E+09	0.3350567E+09	0.1137695E+16	0.1306172E+11	0.7518751E+08
0.8000000E-04	0.2558501E+10	0.6518113E+09	0.3172079E+09	0.1208930E+16	0.1548585E+11	0.1669149E+09
0.9000000E-04	0.2962700E+10	0.4012732E+09	0.2674355E+09	0.1266414E+16	0.1786510E+11	0.3306296E+09
0.1000000E-03	0.3194329E+10	0.9173075E+09	0.1976199E+09	0.1312653E+16	0.1978282E+11	0.5960435E+09
0.1100000E-03	0.3737019E+10	0.9755103E+09	0.1674290E+09	0.1293341E+16	0.2183008E+11	0.9837962E+09
0.1200000E-03	0.4186606E+10	0.9124251E+09	0.1522388E+09	0.1289382E+16	0.2371193E+11	0.1533158E+10
0.1300000E-03	0.2577512E+10	0.2301651E+10	-0.1580738E+09	0.1897654E+16	0.2567973E+11	0.2310910E+10
0.1400000E-03	0.2607416E+10	0.2446462E+10	-0.1867231E+09	0.1595262E+16	0.2901519E+11	0.3106581E+10
0.1500000E-03	0.2875801E+10	0.2294698E+10	-0.1873695E+09	0.1478962E+16	0.3123493E+11	0.3791208E+10
0.1600000E-03	0.2011159E+10	0.2036412E+10	0.5572236E+08	0.2520387E+16	0.3617416E+11	0.4591590E+10
0.1700000E-03	0.2427352E+10	0.2005243E+10	0.7587956E+08	0.2142101E+16	0.3984279E+11	0.5370822E+10
0.1800000E-03	0.3042522E+10	0.1913871E+10	0.1236164E+09	0.1969280E+16	0.4176698E+11	0.6126599E+10
0.1900000E-03	0.3429263E+10	0.1706348E+10	0.1571200E+09	0.2071564E+16	0.4393935E+11	0.7129498E+10
0.2000000E-03	0.4668683E+10	0.1383246E+10	0.1750692E+09	0.1821422E+16	0.4657693E+11	0.8416995E+10
0.2100000E-03	0.5152831E+10	0.1267418E+10	0.1614906E+09	0.1715470E+16	0.4789101E+11	0.1017181E+11
0.2200000E-03	0.9974729E+10	0.5342525E+09	-0.1805641E+09	0.3257567E+16	0.5395775E+11	0.1252731E+11
0.2300000E-03	0.1084243E+11	0.4698294E+09	-0.1849190E+09	0.2578569E+16	0.5909920E+11	0.1660756E+11
0.2400000E-03	0.1045117E+11	0.3846278E+09	-0.1641621E+09	0.2242430E+16	0.6091143E+11	0.2322195E+11
0.2500000E-03	0.1147587E+11	0.1575582E+10	0.9772539E+08	0.2940165E+16	0.6495843E+11	0.3110000E+11
0.2600000E-03	0.1053862E+11	0.1528936E+10	0.9840726E+08	0.2492651E+16	0.6929131E+11	0.4045708E+11
0.2700000E-03	0.1046513E+11	0.1448724E+10	0.6676152E+08	0.2284438E+16	0.7071664E+11	0.5104479E+11
0.2800000E-03	0.2077847E+11	0.1381765E+10	-0.9797440E+08	0.3987883E+16	0.8186590E+11	0.6231219E+11

```

0.2900000E-03 0.1870781E+11 0.1216517E+10 -0.5768957E+08 0.3329451E+16 0.8745701E+11 0.8110183E+11
0.3000000E-03 0.1786551E+11 0.1131935E+10 -0.4741462E+08 0.2990082E+16 0.8917451E+11 0.1083579E+12
0.3100000E-03 0.2696527E+11 0.2155804E+10 -0.3413687E+08 0.5543974E+16 0.1085501E+12 0.1372731E+12
0.3200000E-03 0.2617871E+11 0.2007588E+10 -0.5597005E+08 0.4671377E+16 0.1176654E+12 0.1770357E+12
0.3300000E-03 0.2558772E+11 0.1888965E+10 -0.6616100E+08 0.4191036E+16 0.1208344E+12 0.2312717E+12
0.3400000E-03 0.5197218E+11 0.1403039E+10 -0.8217894E+08 0.8909427E+16 0.1559672E+12 0.2907560E+12
0.3500000E-03 0.4849446E+11 0.1244249E+10 -0.1779618E+09 0.7242581E+16 0.1704684E+12 0.3916602E+12
0.3600000E-03 0.4586957E+11 0.1051886E+10 -0.2228110E+09 0.6376839E+16 0.1752623E+12 0.5463377E+12
0.3700000E-03 0.5984645E+11 -0.6268413E+09 -0.2049988E+09 0.8879196E+16 0.2009981E+12 0.7155596E+12
0.3800000E-03 0.5641468E+11 -0.6148432E+09 -0.1465640E+09 0.7732608E+16 0.2094865E+12 0.9299237E+12
0.3900000E-03 0.5354831E+11 -0.5636524E+09 -0.1091464E+09 0.7010046E+16 0.2105549E+12 0.1200673E+13
0.4000000E-03 0.5532407E+11 -0.3198399E+10 -0.2313693E+09 0.8031406E+16 0.2181677E+12 0.1487184E+13
0.4100000E-03 0.5151282E+11 -0.2724867E+10 -0.2053407E+09 0.7084481E+16 0.2166903E+12 0.1801597E+13
0.4200000E-03 0.4870091E+11 -0.2391400E+10 -0.1894922E+09 0.6435176E+16 0.2117970E+12 0.2139733E+13
0.4300000E-03 0.4402497E+11 -0.3005072E+10 -0.2510577E+09 0.6124948E+16 0.2073344E+12 0.2483757E+13
0.4400000E-03 0.4159552E+11 -0.2617495E+10 -0.2388317E+09 0.5619388E+16 0.2005911E+12 0.2824180E+13
0.4500000E-03 0.3968162E+11 -0.2332918E+10 -0.2328528E+09 0.5218854E+16 0.1930800E+12 0.3157566E+13
0.4600000E-03 0.3769034E+11 -0.2138867E+10 -0.2424562E+09 0.5161521E+16 0.1885192E+12 0.3492546E+13
0.4700000E-03 0.3572359E+11 -0.1930450E+10 -0.2450566E+09 0.4767889E+16 0.1818631E+12 0.3825415E+13
0.4800000E-03 0.3418083E+11 -0.1771244E+10 -0.2416840E+09 0.4457141E+16 0.1744470E+12 0.4156065E+13
0.4900000E-03 0.3566067E+11 -0.1815047E+10 -0.1513804E+09 0.4538198E+16 0.1716677E+12 0.4484427E+13
0.5000000E-03 0.3376991E+11 -0.1618371E+10 -0.1486553E+09 0.4197252E+16 0.1657635E+12 0.4822881E+13
0.5100000E-03 0.3224452E+11 -0.1457500E+10 -0.1426904E+09 0.3943083E+16 0.1589842E+12 0.5174404E+13
0.5200000E-03 0.3091928E+11 -0.1657652E+10 -0.1150365E+09 0.3957174E+16 0.1550423E+12 0.5517396E+13
0.5300000E-03 0.2932115E+11 -0.1516406E+10 -0.1181553E+09 0.3696401E+16 0.1493656E+12 0.5857652E+13
0.5400000E-03 0.2804518E+11 -0.1399122E+10 -0.1193192E+09 0.3484644E+16 0.1430817E+12 0.6191238E+13
0.5500000E-03 0.1738583E+11 -0.2243387E+09 -0.2698766E+09 0.3617058E+16 0.1360162E+12 0.6518241E+13
0.5600000E-03 0.1667264E+11 -0.3081314E+09 -0.2687529E+09 0.3123955E+16 0.1302232E+12 0.6783102E+13
0.5700000E-03 0.1632980E+11 -0.3799611E+09 -0.2679886E+09 0.2883122E+16 0.1241731E+12 0.6942307E+13

```

Appendix C.2 – LS-DYNA Input Keycard Files

We have omitted *mesh.text* because it spans over 13,000 lines and merely lists the coordinates for each rail and the armature mesh, offering little insight. Instead, we will showcase below the *current.k*, *em.k*, *i.k*, and *struc.k* keyword files. In LS-DYNA, these files can be modified either through LS-PrePost’s Keyword Manager (Figure 13) or by editing the files directly, akin to punch-card programming from the 1980s.

```

$# LS-DYNA Keyword file created by LS-PrePost(R) V4.10.5-23Jun2023
$# Created on May-7-2024 (22:36:44)
*KEYWORD
*DEFINE_CURVE
$    LCID      SIDR      SFA      SFO      OFFA      OFFO      DATTYP
$----1-----2-----3-----4-----5-----6-----7-----8
$#    lcid      sidr      sfa      sfo      offa      offo      dattyp    lcint
        4          0       0.001     2000000           0.0         0.0          0          0
$#          a1          o1
          0.0          0.0
          0.08        350.0
          0.2          450.0
          0.4          310.0
          0.6          230.0
          1.0          125.0
*END

```

```

## LS-DYNA Keyword file created by LS-PrePost(R) V4.10.5-23Jun2023
## Created on May-7-2024 (22:36:44)
*KEYWORD
*TITLE
## title
EM Mass-Driver example
*EM_CONTROL
$-----1-----2-----3-----4-----5-----6-----7-----8
$ emsol
$# emsol      numls     macrodt    dimtype    nperio      -   ncylfem   ncylbem
      1        100       0.0        0           2             5000       5000
*EM_CONTROL_CONTACT
$-----1-----2-----3-----4-----5-----6-----7-----8
$ EMcont
$# emct      cconly    ctype      cotype      eps1       eps2       eps3       d0
      1          0         0          0         0.3        0.3        0.3        0.0
*EM_CONTROL_TIMESTEP
$# tstype      dtcons    lcid       factor      tsmin      tsmas      rlcsf      mecats
      1&em_dt            0           1.0        0.0        0.0        25          0
*EM_CIRCUIT_ROGO
$# rogoid      setid      settype    curtyp
      4          4         1           1
*EM_SOLVER_BEMMAT
$# matid      unused     unused     unused     unused     unused     unused     reltol
      1                   unused           unused           unused           1.00000E-6
*EM_SOLVER_BEMMAT
$# matid      unused     unused     unused     unused     unused     unused     reltol
      2                   unused           unused           unused           1.00000E-6
*EM_SOLVER_BEM
$# reltol      maxite     stype      precon     uselast   ncylbem
1.00000E-6      1000       2           2           1&em_bemmtx
*EM_SOLVER_FEM
$# reltol      maxite     stype      precon     uselast   ncylfem
0.001        1000       1           1           1&em_femmtx
*EM_OUTPUT
$ mats      matF      solS      solF      mesh
$# mats      matf      sols      solf      mesh      mem      timing
      2          2         2           2           0           0           0
*EM_DATABASE_GLOBALENERGY
$# outlv      dtout
      1          0.0
*EM_MAT_001
$ em_mid      mtype      sigma     eosId      skinDepth
$# mid        mtype      sigma     eosid      unused     eplambda    deahtt    rdltype
      1          2&em_cond           0           0.01.00000E28      0
*EM_MAT_001
$# mid        mtype      sigma     eosid      unused     eplambda    deahtt    rdltype
      2          2&em_cond           0           0.01.00000E28      0
*EM_MAT_001
$# mid        mtype      sigma     eosid      unused     eplambda    deahtt    rdltype
      3          2&em_cond           0           0.01.00000E28      0
*EM_CIRCUIT
$-----1-----2-----3-----4-----5-----6-----7-----8
$ circid      circtype    lcid

```

```

$#  circid    circtyp      lcid      r/f      1/a      c/t0      v0      t0
      1          3          4      0.55.00000E-5      1.01.500000E8      0.0
$# sidcurr    sidvin    sidvout    partid
      4          1          2          0
*END

$# LS-DYNA Keyword file created by LS-PrePost(R) V4.10.5-23Jun2023
$# Created on May-7-2024 (22:36:44)
*KEYWORD
*TITLE
$#                                         title
EM Mass-Driver example
*PARAMETER
$#     prmr1      val1      prmr2      val2      prmr3      val3      prmr4      val4
R     T_end1e-3
R     dt_plot1e-5
$
$--- EM
$
R     em_dt1e-5
Iem_bemmtx3
Iem_femmtx3
R     em_cond25
$--- STRUC
$
R struc_dt1e-5
Rstruc_rho2.64e-3
R struc_E9.7e+10
R struc_nu0.31
*DATABSE_BINARY_D3PLOT
$#     dt      lcdt      beam      npltc      psetid
&dt_plot          0          0          0          0
*INCLUDE
mesh.k
*INCLUDE
struc.k
*INCLUDE
em.k
*INCLUDE
current.k
*EM_DATABASE_CIRCUIT
$#   outlv      dtout
      1          0.0
*EM_DATABASE_PARTDATA
$#   outlv      dtout
      1          0.0
*END
$# LS-DYNA Keyword file created by LS-PrePost(R) V4.10.5-23Jun2023
$# Created on May-7-2024 (22:36:44)
*KEYWORD
*TITLE
$#

```

```

EM Mass-Driver example
*CONTROL_TERMINATION
$ ENDTIM ENDCYC DTMIN ENDENG ENDMAS
$# endtim endcyc dtmin endeng endmas nosol
&t_end 0 0.0 0.01.000000E8 0
*CONTROL_TIMESTEP
$# dtinit tssfac isdo tslimt dt2ms lctm erode ms1st
    0.0 0.0 0 0.0 0.0 5 0 0
*MAT_ELASTIC
$# mid ro e pr da db not used
    1&struc_rho&struc_e &struc_nu 0.0 0.0 0.0
*MAT_RIGID
$# mid ro e pr n couple m alias
    2&struc_rho&struc_e &struc_nu 0.0 0.0 0.0
$# cmo con1 con2
    1.0 7 7
$#lco or a1 a2 a3 v1 v2 v3
    0.0 0.0 0.0 0.0 0.0 0.0
*MAT_RIGID
$# mid ro e pr n couple m alias
    3&struc_rho&struc_e &struc_nu 0.0 0.0 0.0
$# cmo con1 con2
    1.0 7 7
$#lco or a1 a2 a3 v1 v2 v3
    0.0 0.0 0.0 0.0 0.0 0.0
*PART
$ coil
$#
coil
$ pid secid mid eosid hgid grav adpopt tmid
$# pid secid mid eosid hgid grav adpopt tmid
    1 1 1 0 0 0 0 0
*SECTION_SOLID
$ sid elform
$# secid elform aet unused unused unused cohoff gaskeit
    1 1 0 0 0 0.0 0.0
*PART
$ die
$#
workpiece
$ pid secid mid eosid hgid grav adpopt tmid
$# pid secid mid eosid hgid grav adpopt tmid
    2 1 2 0 0 0 0 0
*PART
$ die
$#
workpiece
$ pid secid mid eosid hgid grav adpopt tmid
$# pid secid mid eosid hgid grav adpopt tmid
    3 1 3 0 0 0 0 2

```